Biomaterials 287 (2022) 121676

Contents lists available at ScienceDirect

Biomaterials

journal homepage: www.elsevier.com/locate/biomaterials

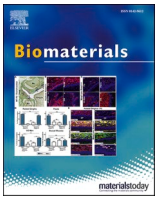

Polyglycerol and Poly(ethylene glycol) exhibit different effects on pharmacokinetics and antibody generation when grafted to nanoparticle surfaces

Kwangsoo Shin [a], Hee-Won Suh [a], Julian Grundler [a,b], Anna Y. Lynn [a], Jinal U. Pothupitiya [a], Zoe M. Moscato [a], Melanie Reschke [a,c], Laura G. Bracaglia [a], Alexandra S. Piotrowski-Daspit [a], W. Mark Saltzman [a,c,d,e,f,*]

[a] Department of Biomedical Engineering, Yale University, New Haven, CT 06511, USA
[b] Department of Chemistry, Yale University, New Haven, CT, 06511, USA
[c] Department of Molecular Biophysics and Biochemistry, Yale University, New Haven, CT, 06511, USA
[d] Department of Chemical & Environmental Engineering, Yale University, New Haven, CT, 06511, USA
[e] Department of Cellular & Molecular Physiology, Yale School of Medicine, New Haven, CT, 06510, USA
[f] Department of Dermatology, Yale School of Medicine, New Haven, CT, 06510, USA

ARTICLE INFO

Keywords:
Polyglycerol
Surface density
Pharmacokinetics
Anti-PEG antibody
Immunogenicity

ABSTRACT

Poly(ethylene glycol) (PEG) is widely employed for passivating nanoparticle (NP) surfaces to prolong blood circulation and enhance localization of NPs to target tissue. However, the immune response of PEGylated NPs—including anti-PEG antibody generation, accelerated blood clearance (ABC), and loss of delivery efficacy—is of some concern, especially for treatments that require repeat administrations. Although polyglycerol (PG), which has the same ethylene oxide backbone as PEG, has received attention as an alternative to PEG for NP coatings, the pharmacokinetic and immunogenic impact of PG has not been studied systematically. Here, linear PG, hyperbranched PG (hPG), and PEG-coated polylactide (PLA) NPs with varying surface densities were studied in parallel to determine the pharmacokinetics and immunogenicity of PG and hPG grafting, in comparison with PEG. We found that linear PG imparted the NPs a stealth property comparable to PEG, while hPG-grafted NPs needed a higher surface density to achieve the same pharmacokinetic impact. While linear PG-grafted NPs induced anti-PEG antibody production in mice, they exhibited minimal accelerated blood clearance (ABC) effects due to the poor interaction with anti-PEG immunoglobulin M (IgM). Further, we observed no anti-polymer IgM responses or ABC effects for hPG-grafted NPs.

1. Introduction

Poly(ethylene glycol) (PEG) has been extensively studied to control the physicochemical properties of implants and particulates and to modulate biochemical interactions in physiological milieu [1–3]. The performance of PEG is singular in nanomedicine. In particular, as a surface coating for various nanoparticles (NPs), it has been shown to reduce nonspecific adsorption of proteins, macrophage uptake, and accumulation in liver and spleen and to prolong blood circulation which increases the chance of NP accumulation in the target tissue [4]. This "stealth" effect of PEG coating enables various NPs to be efficient therapeutic and diagnostic platforms [5].

However, concerns have been raised regarding the immunogenicity of PEGylated nanomaterials. Anti-PEG immunoglobulin M (IgM) antibody (Ab), which is produced after administration of PEGylated drugs or NPs, causes accelerated blood clearance (ABC), leading to loss of therapeutic efficacy of subsequent doses, and can trigger complement activation-related pseudo-allergy (CARPA) [6–10]. Moreover, it has been reported that more than 72% of healthy human blood donors have pre-existing anti-PEG antibodies [11,12]. The loss of efficacy of

Abbreviations: PEG, Poly(ethylene glycol); PG, Polyglycerol; hPG, Hyperbranched polyglycerol; PLA, Polylactide; NP, Nanoparticle; ABC, Accelerated blood clearance; IgM, Immunoglobulin M; AUC, Area under the curve; ELISA, Enzyme-linked immunosorbent assay.

* Corresponding author. Malone Engineering Center, 55 Prospect Street, Room 413, New Haven, CT, 06511, USA.
E-mail addresses: kwangsoo.shin@yale.edu (K. Shin), mark.saltzman@yale.edu (W.M. Saltzman).

https://doi.org/10.1016/j.biomaterials.2022.121676
Received 31 January 2022; Received in revised form 11 June 2022; Accepted 8 July 2022
Available online 11 July 2022

PEGylated therapeutics due to the presence of antibodies has been one of the main challenges toward clinical approval [13–16]. Thus, alternative polymers for NP coating with stealth properties that do not elicit an immune response might overcome these issues, while improving treatment efficacy and reducing allergic reactions induced by treatments involving multiple administrations [17–19]. Many potential PEG alternatives have been developed, including poly(vinylpyrrolidone) (PVP) [20,21], poly(oxazoline) (POx) [22], poly(phosphoester) (PPE) [23], and zwitterionic polymers [24–27]. These hydrophilic polymers have been highlighted for their potential as PEG-alternatives that do not produce polymer specific antibodies or elicit ABC effect even after multiple administrations [21]. Despite the lack of ABC effect, most of the alternative polymers have been shown to be less powerful than PEG in terms of their stealth properties.

Among PEG-alternative polymers, polyglycerol (PG)—composed of the same ethylene oxide backbone as PEG with an additional hydroxymethyl group attached to each repeating unit—has garnered attention in biomedical applications due to its anti-fouling property as well as chemical versatility [28,29]. Specifically, PG has been used as a coating on various nanomaterials enabling distinct stealth behaviors such as evasion of macrophage uptake and enhancement of blood circulation [30–32]. Furthermore, the hydroxyl groups on PG allow it to be modified with multiple functional molecules including drugs, targeting ligands, or contrast agents [33,34]. In addition, the hydroxyl groups at the dendritic chain ends of hyperbranched PG (hPG) can be converted to aldehydes to render PG-grafted NPs bioadhesive and extend the retention of drug-loaded NPs in target tissue [35–37].

Another advantage of PG is its structural versatility based on its variable degree of branching, which allows for tuning of physicochemical properties [38,39]. Although linear PG-grafted therapeutics have been demonstrated to evade ABC [40,41], the impact of the structural differences between PG and PEG on NP coatings has not been systematically studied. Since the stealth and Ab-inducing properties of polymer-grafted NPs are strongly affected by polymer length, end-group, structure, NP size, and the surface density of the grafted polymer [42–46], it is necessary to consider these physicochemical properties to adequately evaluate the performance of each polymer.

In this work, we synthesized linear PG of equivalent backbone length and end-group as methoxy-PEG. Subsequently, we produced polylactide-linear polyglycerol block-co-polymer (PLA-PG) and a hyperbranched PG analog (PLA-hPG), and formed NPs to compare to PLA-PEG NPs, which have been the subject of prior clinical trials [47]. To rule out the effect of NP size on the pharmacokinetic behavior, we prepared NPs with varying surface densities of PEG, PG, and hPG with similar particle size. Furthermore, we evaluated their stealth properties based on protein adsorption, macrophage uptake, pharmacokinetic parameters, and biodistribution. For immunogenicity, we examined anti-PEG antibody generation, antibody binding affinities, and ABC effect. The results from this study broaden our understanding of the relationship of polymeric structure and its role in NP-coating and suggest design considerations for therapeutic NPs of various PEG-alternative compositions to achieve their therapeutic potential in nanomedicine.

2. Materials and methods

2.1. Materials and reagents

2-methoxyethanol (99.8%, anhydrous), potassium tert-butoxide solution (1.0 M in THF), *D,L*-lactide (99%), 1,8-Diazabicyclo[5.4.0]undec-7-ene (DBU, >99%), aluminum chloride hexahydrate (99%), ethyl vinyl ether (99%), *p*-Toluenesulfonic acid (TsOH, 98.5%), poly(ethylene glycol) methyl ether (mPEG, average M_n 5000), calcium hydride, and anhydrous solvents including diglyme (99.5%), tetrahydrofuran (THF, 99.9%, inhibitor free) were purchased from Sigma-Aldrich. Glycidol (96%, Acros Organics), diatomaceous earth (Celite 545 filter aid) and solvents such as methylene chloride (DCM), diethyl ether, tetrahydrofuran (THF), dimethyl sulfoxide (DMSO) were purchased from Fisher Scientific. Deuterated solvents including D_2O, acetonitile-d_3, and DMSO-d_6 were purchased from Sigma-Aldrich. DiI fluorescent dye and microBCA assay kit were purchased from ThermoFisher Scientific. Uniblock poly(*D,L*-lactic acid) was purchased from Lactel Absorbable Polymers.

2.2. Synthesis of ethoxyethyl glycidyl ether

Ethoxyethyl glycidyl ether (EEGE) was synthesized by protecting the hydroxyl group of glycidol. Briefly, glycidol (80 g) and vinyl ethyl ether (400 ml) were mixed in a round-bottom flask and sealed with a septum. After the reaction mixture was cooled to −40 °C in an acetonitrile/dry ice bath, 2 g of TsOH was slowly added to the flask. The solution was stirred overnight, letting the reactor temperature increase to room temperature. The crude product was washed three times with saturated sodium bicarbonate solution in a separation funnel and the organic layer was dried with magnesium sulfate. Residual ethyl vinyl ether was removed using a rotary evaporator and purified EEGE was obtained by vacuum distillation with calcium hydride drying agent.

2.3. Synthesis of PLA-PG block-co-polymer

Synthesis of PLA-PG consists of the following three steps: (1) synthesis of poly(ethoxyethyl glycidyl ether) PEEGE by ring-opening polymerization of EEGE, (2) polymerization of lactides on PEEGE as macroinitiator, and (3) selective deprotection of hydroxyl group on EEGE to convert PEEGE to PG.

2.3.1. Synthesis of PEEGE

To a Schlenk flask with rare earth magnetic stir bar, anhydrous 2-methoxyethanol (1 mmol, 76 mg), potassium tert-butoxide solution dissolved in THF (1 mmol, 1.0 ml), and anhydrous diglyme (1.0 ml) were transferred using syringes under argon atmosphere. The mixture reacted under argon over 20 min at 50 °C. Diglyme was removed via vacuum distillation over 2 h at 80 °C, and the reaction vessel was cooled back down to 50 °C. Additional 2-methoxyethanol (1 mmol, 76 mg) and 1 ml of diglyme were added to the dried flask to obtain a transparent solution. Purified and dried EEGE (220 mmol, 32.2 g) was added dropwise with a syringe pump (1.6 ml·h^{-1}) to minimize self-initiation of monomers and obtain monodisperse polymers with the targeted molecular weight. The reaction proceeded for an additional 24 h and was then allowed to cool to room temperature. Anhydrous THF (32 ml) was transferred to the flask to dilute PEEGE (30 mM) and reduce the viscosity of the polymer solution.

2.3.2. Ring-opening polymerization of lactide on PEEGE

A Schlenk flask with 3.6 g (0.5 mol) of *D,L*-lactide was prepared and purged with argon to obtain an inert atmosphere. Anhydrous THF (60 ml) was transferred to the flask using a cannula and then stirred using a magnetic stirrer. After the lactide was fully dissolved, PEEGE solution in THF was rapidly added to the flask. Depending on the target molecular weight of PLA, the amount of added PEEGE solution was adjusted. For example, for 8 kDa-PLA, 0.45 mmol of PEEGE was used (equivalent to 15 ml of polymer solution). Subsequently, DBU (0.225 mmol, 34 mg) was added to the reaction mixture under argon. The reaction was quenched by adding benzoic acid. The reaction time was determined by monitoring the conversion rate of lactide to PLA calculated from ^{1}H NMR of the reaction mixture. In particular, the reaction time was varied from 30 min to 12 h depending on the amount of macroinitiator and catalyst added. After the reaction, two-thirds of the solvent were removed using a rotary evaporator followed by the addition of methanol to dilute the PLA-PEEGE solution with THF/methanol.

2.3.3. Selective deprotection of hydroxyl group on PG

0.72 mmol of $AlCl_3$ dissolved in methanol (0.2 M) (0.495 mmol (1/100 of [EEGE]) + 0.225 mmol for DBU) was added to the reaction vessel and stirred for 30 min. Subsequently, the crude product was filtered through Celite to remove the acid catalyst. DCM and methanol were used to dissolve and wash out polymer from Celite. The solvent was removed from the filtrate by rotary evaporation and the polymer was precipitated in cold diethyl ether. The precipitate was redissolved in DCM/methanol (5:1) mixed solvent, precipitated in cold diethyl ether, and dried under vacuum.

2.4. Synthesis of mPEG-PLA block-co-polymer

mPEG-PLA block-co-polymers were synthesized by ring-opening polymerization of lactide at room temperature using mPEG as macro-initiator and DBU as catalyst. Prior to polymerization, residual water in mPEG was removed by azeotropic distillation in toluene. Dried mPEG (0.60 mmol, 3.0 g) and lactide (33.4 mmol, 4.8 g) were transferred to a flask and dissolved in 40 ml DCM under argon atmosphere. After the precursors were fully dissolved, DBU (0.3 mmol, 46 mg) was added to the flask. Polymerization was allowed to proceed for 30 min and stopped via addition of benzoic acid (1.0 mmol). The polymer was purified via precipitation in cold diethyl ether, washed three times, and the final product was dried under vacuum. The ratio of initiator, monomer, and catalyst was changed depending on the target molecular weight of PLA.

2.5. Characterization of the polymers

Proton nuclear magnetic resonance (^{1}H NMR) spectra were obtained using an Agilent DD2 400 MHz spectrometer. The molecular weights of all polymers were measured by gel permeation chromatography (GPC) using an Ultimate 3000 UHPLC system (Thermo Fisher Scientific) equipped with a TREX refractive index detector (Wyatt Technologies) and a Malvern CLM1020 column at 50 °C. Dimethylformamide with 1.0 g·L^{-1} of lithium bromide was used as the eluent at a flow rate of 0.4 ml·min^{-1}. Molecular weights were obtained based on the calibration curves from PEG or polystyrene standards (Agilent).

2.6. Preparation of NPs with controlled surface density

PLA-PEG and PLA-PG NPs were prepared by nanoprecipitation. Briefly, polymer solutions dissolved in 50% acetonitrile and 50% methanol (v/v) were prepared with different composition of uniblock PLA and diblock-co-polymer (PLA-PEG or PLA-PG) and added dropwise to 3–7 ml of water under stirring. The ratio of polymers was controlled to obtain the desired size and surface density, adapted from published reports [42]. To afford uniform NPs, the polymers should be fully dissolved in organic solvent. Since PLA-PG cannot be fully dissolved in acetonitrile, a polar solvent such as methanol was also added to the polymer solution before nanoprecipitation. PLA-hPG was prepared following a previously published method [30]. PLA-hPG NP1 was prepared in the same manner as PLA-PEG and PLA-PG via nanoprecipitation. PLA-hPG NP2 was prepared by a single emulsion method using ethyl acetate as the immiscible organic solvent to form uniform NPs. To prepare fluorescent NPs, DiI solution (DMSO, 10 mg·ml^{-1}) equivalent to 0.3 wt% of polymer was added to the polymer solution. Additional details of the NP preparation methods are described in Table S3 and S4.

2.7. Characterization of NPs and calculation of surface density

Hydrodynamic size and ζ-potential were measured using a Malvern Zetasizer nano ZS. To quantify the percentage of solvated hydrophilic polymer (PEG, PG, hPG) on the NP surface, NPs in H_2O were washed with D_2O containing internal standard (0.75 wt% trimethylsilyl propanoic acid, TMSA) four times using filter centrifugation (Amicon® Ultra-2 Centrifugal Filter Unit, MWCO 100 kDa, 2 ml, Millipore).

After obtaining ^{1}H NMR spectra, the solutions were transferred to vials and 2-fold of DMSO-d_6 and 1-fold of acetonitrile-d_3 were added in order to fully dissolve the hydrophobic PLA core. The dissolved polymer solution was then analyzed via ^{1}H NMR again. To calculate the exposure ratio, the relative integration of PEG/PG/hPG to TMSA obtained in D_2O was divided by the relative integration of fully dissolved polymers to TMSA. The weight ratio of hydrophilic polymers in NPs were quantified from the spectra of fully dissolved polymers solution. By multiplying the exposure ratio to the weight ratio, exposed PEG/PG/hPG wt% can be evaluated.

The surface density of hydrophilic polymer on NPs was calculated using the following equation, published elsewhere [42].

$$PEG(PG)surface\ density = \frac{exposed\ PEG(PG)wt\% \times V \times \rho \times N_A}{PEG(PG)MW \times S}$$

Z-average dynamic light scattering (DLS) size was used to calculate average surface area (S) and volume (V). The weight ratio and percent of exposed hydrophilic polymer was evaluated by ^{1}H NMR to calculate the average number of polymers per NP. The density (ρ) of polymeric particles was estimated as 1.2 g·cm^{-3}. N_A is Avogadro's number.

2.8. Cryo-transmission electron microscopy (TEM) imaging of NPs

Quantifoil holey carbon 300 mesh copper grids (Electron Microscopy Sciences) were glow-discharged to render them hydrophilic using a PELCO easiGLOW. A FEI Vitrobot cryo plunger (ThermoFisher Scientific) was used to vitrify NPs (20 mg·ml^{-1} in water, 3.5 μl per grid) in liquid ethane. Sample grids were stored in liquid nitrogen and transferred to a cryo grid holder (Gatan 626) for imaging. After inserting the grid holder into a FEI Talos L120C (ThermoFisher Scientific) TEM operated at an acceleration voltage of 120 kV, cryo-TEM were obtained under low dose conditions at −2 μm defocus.

2.9. Protein adsorption using microBCA assay

1 ml of NP solution (2 mg·ml^{-1}, phosphate buffered saline (PBS) pH 7.4) was mixed with fetal bovine serum (FBS) and gently shaken at 37 °C for 1 h. The mixture was centrifuged for 1 h at 20,000 g and 4 °C, and pellets were washed three times with PBS. To release protein adsorbed to the NP surface, the pellets were resuspended in 50 μl surfactant buffer (4% Triton X-100 and 2% sodium dodecyl sulfate) and sonicated for 15 min. A MicroBCA protein assay kit (ThermoFisher, USA) was used to analyze the protein concentration. The standard curve for the microBCA assay was obtained using bovine serum albumin (BSA) standards diluted with PBS containing lysis buffer at the same final concentration as the samples.

2.10. LC-MS/MS analysis of proteins corona adsorbed on NPs

To obtain the murine plasma, blood collected with an EDTA-coated tube from 6-week old female BALB/c mice was centrifuged for 30 min at 8000 g at 4 °C. NPs (5 mg) in solution at 50 mg·ml^{-1} were mixed with 500 μl of collected plasma and incubated at 37 °C while shaking at 120 rpm for 1 h. NPs and adsorbed proteins were collected, washed with PBS two times, and pelleted by centrifugation for 6 h at 20,000 g at 4 °C. After the NPs were resuspended in distilled water, 0.5 ml acetone and 1 ml of acetonitrile were added to fully dissolve NPs and precipitate proteins. The samples were spun for 30 min at 3000 g at 4 °C and supernatant containing polymer removed. The remaining protein pellets were washed twice with cold acetonitrile and dissolved in ammonium bicarbonate buffer (50 mM) containing 1% sodium deoxycholate. The protein samples were sent to Yale Mass Spectrometry & Proteomics Resource of the W.M. Keck Foundation Biotechnology Resource Laboratory for mass spectrometry analysis.

2.10.1. In solution protein digestion

Protein samples dissolved in 50 mM ammonium bicarbonate with 1% sodium deoxycholate were concentrated by SpeedVac to 100 μl (~3 fold). The proteins were reduced by the addition of 1/10 volume of 45 mM dithiothreitol (Thermo Scientific) and incubation at 37 °C for 30 min, cooled to room temperature, then alkylated with the addition of 1/10 volume of 110 mM iodoacetamide (Sigma-Aldrich) with incubation in the dark at room temperature for 30 min. Proteins were then acetone precipitated at −20 °C overnight using standard protocols. Protein pellets were dissolved and denatured in 8 M urea, 0.4 M ammonium bicarbonate, pH 8. The urea concentration was adjusted to 2 M by the addition of water prior to enzymatic digestion at 37 °C with trypsin (Promega) for 3 h, followed by an additional addition of trypsin prior to overnight digestion at 37 °C. Samples were acidified by the addition of 1/40 volume of 20% trifluoroacetic acid, then desalted using BioPureSPN Mini PROTO 300C18 columns (The Nest Group) following the manufacturer's directions with peptides eluted with 0.1% TFA, 80% acetonitrile. Eluted peptides were speedvaced dry and dissolved in MS loading buffer (2% acetonitrile, 0.2% trifluoroacetic acid). A nanodrop measurement (Thermo Scientific Nanodrop 2000 UV–Vis Spectrophotometer) determined protein concentrations (A260/A280). Each sample was then further diluted with MS loading buffer to 0.06 μg·μl $^{-1}$, with 0.3 μg (5 μl) injected for LC-MS/MS analysis.

2.10.2. LC-MS/MS on the Thermo Scientific Q Exactive Plus

LC-MS/MS analysis was performed on a Thermo Scientific Q Exactive Plus mass spectrometer equipped with a Waters nanoAcquity UPLC system utilizing a binary solvent system (A: 100% water, 0.1% formic acid; B: 100% acetonitrile, 0.1% formic acid). Trapping was performed at 5 μl·min^{-1}, 99.5% Buffer A for 3 min using an ACQUITY UPLC M-Class Symmetry C18 Trap Column (100 Å, 5 μm, 180 μm × 20 mm, 2G, V/M; Waters, #186007496). Peptides were separated at 40 °C using an ACQUITY UPLC M-Class Peptide BEH C18 Column (130 Å, 1.7 μm, 75 μm × 250 mm; Waters, #186007484) and eluted at 300 nl·min^{-1} with the following gradient: 3% buffer B at initial conditions; 5% B at 2 min; 25% B at 140 min; 40% B at 165 min; 90% B at 170 min; 90% B at 180 min; return to initial conditions at 182 min. MS was acquired in profile mode over the 300–1700 *m/z* range using 1 microscan, 70,000 resolution, AGC target of 3E6, and a maximum injection time of 45 ms. Data dependent MS/MS were acquired in centroid mode on the top 20 precursors per MS scan using 1 microscan, 17,500 resolution, AGC target of 1E5, maximum injection time of 100 ms, and an isolation window of 1.7 *m/z*. Precursors were fragmented by HCD activation with a collision energy of 28%. MS/MS were collected on species with an intensity threshold of 1E4, charge states 2–6, and peptide match preferred. Dynamic exclusion was set to 30 s.

2.10.3. Peptide identification and data processing

Data was analyzed using Proteome Discoverer software v2.5 (Thermo Scientific). Data searching was performed using the Mascot algorithm (version 2.8.0) (Matrix Science) against the SwissProt database with taxonomy restricted to *Mus musculus* (17,114 sequences). The search parameters included tryptic digestion with up to 2 missed cleavages, 10 ppm precursor mass tolerance and 0.02 Da fragment mass tolerance, and variable (dynamic) modifications of methionine oxidation and carbamidomethyl cysteine. Normal and decoy database searches were run, with the confidence level set to 95% ($p < 0.05$). Scaffold (version Scaffold_5.0, Proteome Software Inc.) was used to validate MS/MS based peptide and protein identifications. Peptide identifications were accepted if they could be established at greater than 95.0% probability by the Percolator posterior error probability calculation. Protein identifications were accepted if they could be established at greater than 99.0% probability and contained at least 2 identified peptides. Top 100 abundant identified proteins were presented and used to calculate the normalized compositions.

2.11. Cellular uptake of NPs

Murine macrophage cells RAW 264.7 purchased from ATCC were thawed and cultured in a T75 flask containing Dulbecco's Modified Eagle's Medium (DMEM) with 10% FBS and 1% penicillin/streptomycin (P/S) at 37 °C in a 5% CO_2 humidified atmosphere. To 24-well tissue culture plates, 0.5 ml of cell suspension (10^5 cell·ml^{-1}) was added to each well and incubated for 24 h. The original DMEM medium was replaced with fresh culture medium containing 200 μg·ml^{-1} of fluorescent NPs. The cells were further incubated at 37 °C for 24 h and rinsed three times with cold sterile PBS. After treatment with trypsin, the cells were collected, resuspended in FACS buffer (2% BSA in PBS), and run directly on the flow cytometer (Attune NxT).

2.12. Pharmacokinetic analysis

All animal procedures were performed in accordance with the guidelines and policies of the Yale Animal Resource Center and approved by the Institutional Animal Care and Use Committee of Yale University. Female C57Bl/6J mice aged 6- to 8-weeks old were purchased from Jackson Laboratory. Mice were anesthetized using an isoflurane chamber. Fluorescent NPs (20 mg·kg^{-1}) were intravenously administered via retro-orbital injection and a small tail nick was made with a sterile blade. The concentrations of NPs in blood were obtained by employing a high-throughput quantitative microscopy-based half-life measurement which has been previously published [48]. Briefly, 2 μl of blood samples were collected at 0.5, 1, 2, 4, 8, 12, 24, and 48 h after administration with a micropipette from the tail nick. Collected blood samples were diluted in pre-made solution containing 2 μl of heparin solution (1000 USP·ml^{-1}) and 8 μl of PBS in heparinized tube, followed by flash-freezing on dry ice. A calibration curve was obtained by spiking heparin solutions containing freshly collected blood from non-treated mice with a known concentration of NP solution followed by serial dilution from 0 to 500 μg·ml^{-1} of NPs. The diluted blood samples and standards were transferred to a 384-well plate and imaged with an EVOS FL Auto 2 Cell Imaging System, with standard RFP filters and Olympus superapochromat 20×/0.75 NA objective. Images were processed to obtain mean fluorescence intensity and these values were converted to concentration of NPs using a standard curve.

Pharmacokinetic parameters were calculated using non-compartmental analysis. Area under the concentration-time curves (AUC_{0-48h}) were calculated via the trapezoidal method from 0 to 48 h. The half-life ($t_{1/2}$) and elimination rate (k_e) were assessed by non-linear first order exponential decay fitting of the blood concentration vs time curve from 30 min to 48 h time point. The apparent initial concentration (C_0) was determined from the y-intercept of the first order exponential decay curve.

2.13. Endothelial cell adsorption of NPs

Human umbilical vein endothelial cells (HUVECs) were obtained from the Yale Vascular Biology and Therapeutics tissue culture core. HUVECs pooled from three donors were isolated from fresh umbilical veins by collagenase digestion and cultured on 0.1% gelatin-coated flasks containing M199 medium (Gibco) supplemented with 20% FBS, 1% P/S, and 1% endothelial cell growth supplement. To 96-well tissue culture plates coated with gelatin, 0.1 ml of cell suspension (10^5 cell·ml^{-1}) was added to each well and incubated for 24 h. The medium was replaced with 100 μl of NPs solution (2.5 mg·ml^{-1}) dispersed in PBS containing different FBS concentration (0%, 10%, 25%, 50%). To quantify association of NPs with cellular membrane rather than phagocytosis and micropinocytosis, NP solutions were removed after 5 min of incubation, and rapidly rinsed with Hank's balanced salt buffer three times. The cells were detached from well plate by TrypLE (Gibco), collected, and resuspended in FACS buffer (2% BSA in PBS), and run directly on the flow cytometer (Attune NxT).

2.14. Biodistribution

After blood collection at the 48 h time point, the animals were sacrificed and perfused transcardially with heparinized PBS (10 U·ml^{-1}). Organs (lungs, liver, spleen, and kidneys) were harvested and stored below −70 °C. Whole lungs, spleen, kidneys, and 200–300 mg of liver tissue were homogenized separately by a Precellys® tissue homogenizer. To a 2 ml size bead tube, 1 ml of 5 wt% Triton-X solution and 500 μl of ethyl acetate (EA) were added together for simultaneous extraction. After centrifuging the tubes (10 min, 20,000 g), 300 μl of the clear top EA layer containing hydrophobic fluorescent dye (DiI) and Triton-X were collected and transferred to a clean tube. EA was evaporated using a vacuum concentrator for 1 h and 500 μl of DMSO was added to the tube to dissolve DiI completely.

Two of each group of organs (lungs, liver, spleen, and kidneys) were collected from control mice, and 5 μg (1 ID%, 10 μl) of NPs were added to one group (positive control). Both control organ groups and treated organs were handled in the same manner. 200 μl of DMSO containing extracted dye and lipophilic tissue lysate was transferred to 96-well plates for measurement of the fluorescence intensity. Standard curves of dye were obtained from serial dilution (1 μg·ml^{-1} to 0.24 ng·ml^{-1}) in DMSO containing Triton-X (6 wt%). The fluorescent intensities of samples and positive control groups were subtracted from the fluorescent intensity of negative control group with auto-fluorescent lipophilic lysate. The dye concentrations extracted from sample tissue and control tissue were calculated from the corrected fluorescence intensity using the standard curve.

To minimize the differences in extraction efficiency and actual encapsulation ratio among NPs, NP amount in tissue was converted using the conversion factor described below.

$$NP\ in\ tissue = concentration\ of\ dye\ extracted\ from\ sample\ tissue \times conversion\ factor$$

$$Conversion\ factor = \frac{Amount\ of\ NPs\ added\ in\ control\ (5\ \mu g)}{concentration\ of\ dye\ extracted\ from\ control\ tissue}$$

Since the DiI dye is extremely hydrophobic, single extraction was enough to collect more than 99.5% of the initial concentration. The dye concentration in the top layer was proportional to the amount of NP added, allowing cacluation of the total amount of dye.

2.15. Quantification of Anti-PEG IgM antibodies

The concentration of anti-PEG IgM antibodies was assessed with an ELISA kit (Mouse Anti-PEG IgM Mouse ELISA kit, PEGM-1, Life Diagnostics Inc.) following the manufacturer's protocol. Mice were anesthetized using an isoflurane chamber before blood collection. Around 50 μl of blood were collected from the retro-orbital sinus using a capillary tube and transferred to a 1.6 ml-tube and clotted for over 10 min at room temperature. The serum was obtained after centrifugation at 8000 *g* and diluted 1000-fold. Each diluted sample and anti-PEG IgM standards were transferred and incubated in an ELISA plate for 1 h on an orbital shaker at room temperature. After washing the wells 5 times, anti-mouse IgM HRP were added as described in the manufacturer protocol. After 30 min, the plate was washed again and TMB reagent was added to each well for 20 min with gentle shaking in the dark. The color development was stopped with the addition of stop reagent. The absorbance of each well was read at 450 nm with a plate reader and the concentration of anti-PEG IgM antibody was calculated using a standard curve.

2.16. ELISA with polymer-coated well

PLA_{8k}-PEG_{5k} and PLA_{8k}-PG_{8k} were completely dissolved with acetonitrile and methanol (5 mg·ml^{-1}). 50 μl of polymer solution were added to a 96-well plate and dried in a vacuum oven at 50 °C. Next, 200 μl of blocking buffer (1% BSA, 50 mM Tris/HCl pH 8.0, 0.14 M NaCl) were added and incubated over 1 h. TBS (50 mM Tris/HCl pH 8.0, 0.14 M NaCl) without surfactant was used to wash the well-plate three times. After preparation of the polymer coated well plates, ELISAs were conducted using the same protocol and reagents described above, except with a different dilution factor (1:500). To verify polymer-coating on plate wells, various concentrations of anti-PEG IgM standards (PEGM-1, Life Diagnostics Inc.) and isotype mice IgM controls (ThermoFisher) were analyzed.

2.17. Competitive ELISA

PLA-PEG NP3, PLA-PEG NP5, methoxy-PEG_{5k}, PLA-PG NP3, PLA-PG NP5, PG_{8k} were incubated in dilution buffer containing anti-PEG IgM standard (10 U·ml^{-1}) for 15 min at different final concentrations of PEG and PG. The solution was added to BSA-PEG coated plates (Life Diagnostics Inc.) and an anti-PEG ELISA was conducted as described above. Identical concentrations of anti-PEG IgM standard solutions without competitor were used as control for normalization. The serum of mice immunized with PLA-PEG NP5 or PLA-PG NP5 were collected, diluted, and incubated with PLA-PEG NP5, PLA-PG NP5, or PLA-hPG NP2 at different hydrophilic polymer concentration followed by ELISA conducted in the same manner.

2.18. Animal study on accelerated blood clearance (ABC)

Male BALB/C mice aged 8 weeks were ordered from Jackson Laboratory. To induce anti-PEG antibody generation and accelerated blood clearance, non-fluorescent NPs (1, 5, 10, or 20 mg·kg^{-1} of doses for PLA-PEG NP5 and PLA-PG NP5 and 10 mg·kg^{-1} dose for PLA-PEG NP3, PLA-PG NP3, and PLA-hPG NP2) were prepared and administered. After 7 days, the serum was collected, and the concentration of anti-PEG IgM antibodies was measured. The same dose of fluorescent NP solutions were administered (1, 5, or 10 mg·kg^{-1}), and pharmacokinetics were assessed as previously described. The ratio of anti-PEG IgM and NPs was calculated using the weight-averaged molar mass of NPs obtained by static light scattering (Dawn Heleos II, Wyatt Technology).

2.19. Statistical analysis

Results were analyzed using Origin (version 2020b 64-bit). Data are presented as mean ± standard deviation (SD) of at least three independent experiments. One-way ANOVA with Tukey's multiple comparisons test was used where appropriate. Values were considered significantly different at $p < 0.05$.

3. Results and discussion

3.1. Synthesis and characterization of PLA-PG block-co-polymer

Synthesis of PLA-PG was performed in three steps: (1) synthesis of poly(ethoxyethyl glycidyl ether) (PEEGE), (2) polymerization of lactides on PEEGE as macroinitiator, and (3) selective deprotection of hydroxyl group on EEGE to convert PEEGE to PG (Fig. S1). We synthesized PG with a similar degree of polymerization (DP) as 5 kDa PEG, a common molecular weight of PEG in biomedical applications for polymeric NP coating, since 5 kDa PEG has been repeatedly shown to enhance the blood circulation half-life of NPs compared to other molecular weights [44,49,50].

The synthesis of linear PG was performed by ring-opening polymerization with ethoxyethyl glycidyl ether (EEGE, hydroxyl group-protected glycidol) as a monomer, which prevented the formation of branches during chain propagation. To directly compare linear PG to methoxy-PEG, we chose 2-ethoxymethanol as the initiator. The molecular weight and polydispersity of PEEGE was controlled by adapting

previously published synthetic methods [51,52]. After the deprotection of acetal groups on PEEGE, PG was obtained with a DP of 100, similar to 5 kDa PEG with a DP of 113. Gel permeation chromatography (GPC) results showed that the size of PEG and PG are comparable with both exhibiting a narrow molecular weight distribution ($Đ < 1.15$, Table S1). PLA-PG was synthesized with PEEGE as a macroinitiator via ring-opening polymerization. A mild Lewis acid (aluminum chloride in methanol) was used for the deprotection of hydroxyl groups on PG to prevent the degradation of PLA by acid-mediated hydrolysis (Fig. S2) [53]. To prepare a series of NPs with controlled surface density and size, PLA-PG and PLA-PEG were synthesized with three different lengths of PLA and characterized by ^{1}H NMR spectroscopy and GPC (Fig. S3, Table S1).

3.2. Preparation and characterization of PLA-PEG NPs, PLA-PG NPs, and PLA-hPG NPs

We prepared a library of 90 nm-sized NPs with varying surface densities of PEG or PG via a previously reported co-precipitation method using a mixture of amphiphilic block-co-polymer (PLA-PEG or PLA-PG) and hydrophobic homopolymer (PLA) (Table S2, S3, and Fig. 1) [42,54]. In total, five different formulations of PLA-PEG NPs and PLA-PG NPs with varying PEG/PG contents were prepared. The average hydrodynamic sizes (D_h) were all within 80–100 nm (Fig. 1D). To probe the influence of surface coverage, stealth property, and immunogenicity caused by structural differences of PG, two PLA-hPG NPs were also prepared and characterized (Fig. 1B, Table S3). The PLA-hPG block-copolymer was synthesized by conjugating PLA to hPG, and PLA-hPG NP2 was prepared by single emulsion method, according to our prior reports [30]. PLA-hPG NP1 was prepared by nanoprecipitation with PLA homopolymer to obtain NPs with less hPG on the NP surface. Surface zeta potentials of all NPs were slightly negative ranging from −25 mV to −10 mV and trended toward neutral with greater PEG or PG surface coverage (Fig. S4). In addition, cryo-TEM imaging confirmed that all of the NPs (PLA-PEG, PLA-PG, and PLA-hPG) were spherical in shape (Fig. S5).

The surface density of hydrophilic polymer on each NP preparation was calculated based on the amount of PEG/PG/hPG exposed on the NPs surface in aqueous suspension by ^{1}H NMR spectroscopy (Fig. 1C). Since the solid PLA core and any embedded PEG/PG/hPG cannot be detected in ^{1}H NMR, we were able to selectively obtain signals from the solubilized hydrophilic polymer corona of the NPs suspended in D_2O. The NMR spectra of NPs in D_2O were compared to respective spectra of NPs fully dissolved by addition of organic solvent (acetonitrile-d_3 and DMSO-d_6) to quantify the exposed hydrophilic polymer with respect to that incorporated in NPs (Fig. S5). The exposure ratio, the fraction of hydrophilic polymer exposed on the NP surface, was evaluated by comparing relative intensities of hydrophilic polymer of both ^{1}H NMR spectra (Fig. 1E).

Due to the solubility differences of PLA versus PG/PEG in water and the self-assembly process during nanoprecipitation, more than 80% of PEG and PG was found to be exposed in the corona for all PLA-PEG and PLA-PG NPs. Interestingly, PLA-hPG NP1 prepared by nanoprecipitation showed a lower exposure ratio of 67%, whereas the exposure ratio for PLA-hPG NP2 prepared via single emulsion method was 83%, indicating more favorable orientation of hPG toward the aqueous phase. It is possible that the bulky and inflexible hPG dendrimers are prone to being trapped inside the NP core during the rapid formation of NPs by nanoprecipitation, resulting in a significant amount of hPG not being fully exposed outward as a corona. The exposed PEG and PG contents in the NPs strongly correlated with the initial wt% of polymer precursor used in nanoprecipitation (Fig. 1F), suggesting that linear hydrophilic polymers, which are flexible, may prefer to be oriented outwards during nanoprecipitation. The surface density was quantified according to previous publications, based on the size of NPs, molecular weight of hydrophilic polymer, and weight percentage of exposed hydrophilic polymers obtained from ^{1}H NMR [42,55,56]. The surface density of PEG and PG on NPs varied between 10 and 60 polymer chains per 100 nm^2 and the surface density of hPG dendrimers on NPs varied between 28 and 44 per 100 nm^2 (Fig. 1G).

In addition, we prepared PLA-PG and PLA-PEG NPs of smaller and larger sizes to compare the effect of PG and PEG on pharmacokinetics in

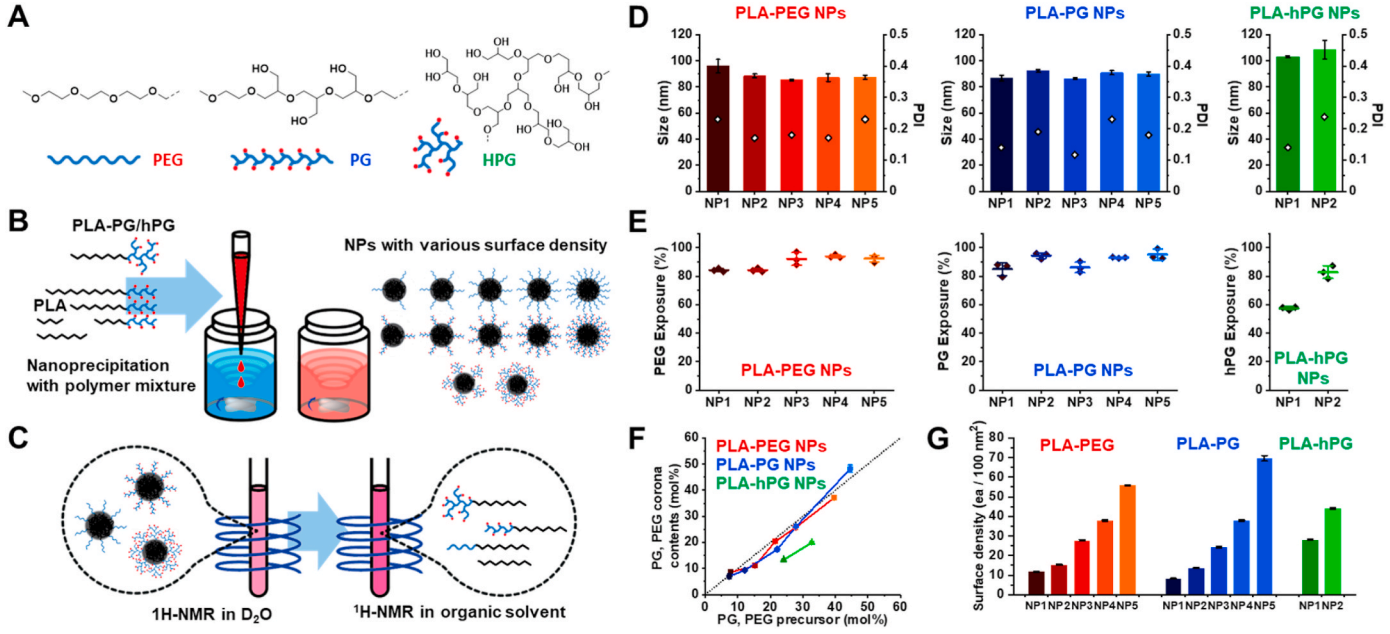

Fig. 1. Preparation and characterization of PEG- or PG-grafted PLA NPs having various polymer surface density. (A) Structure of grafting polymers PEG, PG, and hPG. (B) Fabrication of PLA-PEG, PLA-PG, and PLA-hPG NPs via nanoprecipitation with PLA-PEG, PLA-PG, PLA-hPG, with varying amounts of PLA. (C) Quantification of surface polymers using ^{1}H NMR spectroscopy in different solvents. (D) Size of PLA-PEG NPs (left), PLA-PG NPs (middle), and PLA-hPG NPs (right). (E) Exposure ratio of PEG (right), PG (middle), and hPG (right) in the corona. (F) Analysis of surface polymer contents incorporated in NPs using ^{1}H NMR spectroscopy depending on the contents of PEG, PG, and hPG in the polymer precursor. (G) Surface density of PEG, PG, or hPG in respective NPs.

different NP size regimes (Table S4, Fig. S6). NP of approximately 40 nm in size (PLA-PEG-s and PLA-PG-s) were prepared by nanoprecipitation without additional PLA homopolymer. Conversely, by increasing the amount of PLA homopolymer, we were able to obtain NPs close to 150 nm in size (PLA-PEG-L and PLA-PG-L). The surface densities of small NPs (39 PEG per 100 nm^2 for PLA-PEG-s, 26 PG per 100 nm^2 for PLA-PG-s) and large NPs (26 PEG per 100 nm^2 for PLA-PEG-L, 15 PG per 100 nm^2 for PLA-PG-L) are in the same range as that of the 90-nm sized NPs (10–60 per 100 nm^2).

3.3. Protein adsorption and cellular uptake

As a representative indicator of the stealth property of polymeric coating on NPs, prevention of protein adsorption and antifouling effect was evaluated [57–59]. After incubation of NPs in fetal bovine serum (FBS), the total amount of protein adsorbed onto NPs was analyzed. Similar to the results in the literature, higher PEG surface density resulted in less protein adsorption with smaller differences for NPs with denser PEG coronas (Fig. S7) [54,58–60]. This nonlinear trend was also observed for PG-grafted NPs. Fewer serum proteins adsorbed onto PLA-PG NPs compared to PLA-PEG NPs at low surface density (10 chains per 100 nm^2), however at high surface density, PLA-PEG NPs showed less protein adsorption than PLA-PG NPs.

The composition of proteins on the NP surface has emerged as a dominant factor in the pharmacokinetics of NPs [61,62], since the proteins adsorbed on NPs are known to be key for opsonization or immune cell recognition [42,63]. Even though the total amount of protein adsorbed on NPs is an indicator of a polymer's anti-fouling effect, the composition and adhesion of complement proteins and immunoglobulins are also important to understand the stealth property and its contribution to pharmacokinetics [58]. To further characterize the effect of PEG, PG, and hPG on the NP surface, we examined the protein corona on NPs with different densities of PEG, PG, or hPG (Table S5). The composition of adsorbed proteins was categorized by function and molecular weight (Fig. S9); the surface density of grafted polymers affected the protein ratios more than the identity of grafted polymer. The fraction of apolipoproteins adsorbed on PLA-PEG and PLA-PG NPs decreased as the density of PEG or PG on the NP surface increased. PEG and PG were equally effective in decreasing apolipoprotein adsorption (Fig. S10A). PLA-hPG NP2 exhibited the lowest ratio of apolipoprotein among all samples. This is consistent with the amphiphilic nature of apolipoproteins, resulting in more adsorption on bare hydrophobic PLA surfaces than on surfaces coated with stealthy polymers [42,61].

The adsorption of complement proteins and immunoglobulins is also potentially important, because of their role in recognition by immune cells and NP clearance. The ratio of immunoglobulins did not change significantly with PEG or PG surface density, but PLA-hPG NP2 had a significantly higher level of immunoglobulin adsorption (Fig. S10C). Complement protein adsorption was significantly higher for PLA-PG NP1 and PLA-hPG NP2 than any of the other NPs. Interestingly, for linear PG grafted on the NP surface at a density higher than 20/100 nm^2, the ratio of complement proteins adsorbed on PLA-PG NPs was similar to that on PLA-PEG NPs (Fig. S10B). For PLA-PEG NP5 and PLA-PG NP5, which had the highest density of linear polymers grafted, the ratios of immunoglobulin and complement proteins adsorbed were slightly greater than for NPs with lower PG or PEG density.

Specifically analyzing the composition of each adsorbed protein between PEG and PG NPs showed that the difference among adsorption ratios of individual proteins was largest at the lowest surface density of PEG or PG (Fig. S11A); their compositions became similar as more linear polymers were grafted on NPs surface. Apolipoprotein E, which has been suggested to act as a dysopsonin on NPs [61], was found slightly more in PLA-PEG NPs than PLA-PG NPs, especially when the surface densities of grafted polymers were low (NP1 and NP3). The adsorption of clusterin, which has also been shown to act as a dysopsonin on NPs [64], was reduced at high surface densities of both PEG and PG-grafted NPs, following the decrease in overall apolipoprotein.

Complement component 3 (C3), which plays an important role in the opsonization of nanoparticles, was adsorbed highest among the complement group protein in all NP groups. PLA-PG1 and PLA-hPG NP2 showed a significantly higher level of C3 and other complement proteins adsorbed when compared to other NPs. This could be attributed to the hydroxyl groups on the hPG and PG causing complement proteins to bind [63]. However, the composition of complement proteins was almost identical when comparing PLA-PG NP3 and PLA-PG NP5 to PLA-PEG NP3 and PLA-PEG NP5. We observed that the most densely PG-grafted NPs were similar to PEGylated NPs in terms of protein corona, but PLA-hPG NPs exhibited more complement proteins and immunoglobulins adsorbed on NP surface, which possibly leads to more rapid clearance of PLA-hPG NPs than NPs grafted with PEG or PG.

One of the main clearance pathways of NPs in blood is through the mononuclear phagocyte system (MPS). Thus, the study of NP uptake by macrophages is another measure of the stealth property of polymer coatings. Since the uptake of NP by macrophages and their clearance *in vivo* can be evaluated with long-term incubation over 6 h [65], we analyzed the internalization of NPs by murine macrophages (RAW 264.7) *in vitro* (Fig. S8) by incubating NPs for 24 h. Flow cytometry analysis showed that the NPs with the lowest surface density (PLA-PEG NP1 and PLA-PG NP1) were readily internalized. However, once the surface density reached a certain threshold (>12 PG or PEG/100 nm^2), endocytosis was strongly inhibited, in agreement with previous studies on PEG surface density [54,58]. Above the threshold, the internalization of PG-grafted NPs was similar to that of PEGylated NPs.

3.4. Pharmacokinetic analysis

The blood circulation profiles of dye-loaded NPs were monitored over 48 h by collecting blood samples after intravenous injection into healthy C57BL/6J mice (Fig. 2, Fig. S9). Following the trends observed in the macrophage uptake study, NPs with the lowest surface density (PLA-PEG NP1 and PLA-PG NP1) were most rapidly cleared. We observed longer circulation for NPs with higher surface density. For PEGylated NPs, the half-life of NPs with surface densities over 15 PEG per 100 nm^2 was approximately 12 h, consistent with previous results reported for poly(lactic-co-glycolic acid) (PLGA)-PEG NPs [42]. All parameters, including blood half-life, area under the concentration-time curve (AUC), and elimination constant (k_e), remained within a similar range for NPs with >15 PEG per 100 nm^2. In contrast, blood half-lives and elimination constants of PLA-PG NPs increased steadily with increasing PG surface density, resulting in longer blood circulation than PEGylated NPs with 66 PG per 100 nm^2 (Fig. 2D). However, the AUC of PLA-PG NPs was nearly half that of PLA-PEG NPs, and only slightly increased as the surface density increased from PLA-PG NP2 (750 ID%·h) to PLA-PG NP5 (885 ID%·h) (Fig. 2E). Pharmacokinetic parameters of PLA-hPG NP1 were similar to those of PLA-PG NP1 and PLA-PEG NP1, despite its higher surface density (28 hPG/100 nm^2 compared to ~10 PG or PEG/100 nm^2), but PLA-hPG NP2 exhibited longer circulation with an AUC close to that of PLA-PG NP4, suggesting that a higher density of hPG is necessary to endow a similar degree of stealth property. This may be due to the low conformational flexibility of hPG, which makes it less effective as a surface coating at low density than its linear counterpart in terms of surface coverage and stealthiness [38,65].

PLA-PG NPs exhibited a substantially reduced AUC with a surface density similar to PLA-PEG NPs, despite having comparable circulation half-lives. Notably, the apparent initial concentration C_0, determined from the y-intercept of the of the first order exponential decay curve, was 50% lower for PLA-PG NP3 compared to PLA-PEG NP3 (Fig. 2G). The reduction of NP concentration in blood occurred within 5 min after administration, which is an extremely short period to be explained by clearance via macrophage uptake. We reasoned that the NP-solution administered encounters endothelial cells while they are mixed with the serum proteins during distribution phase and hypothesized that the

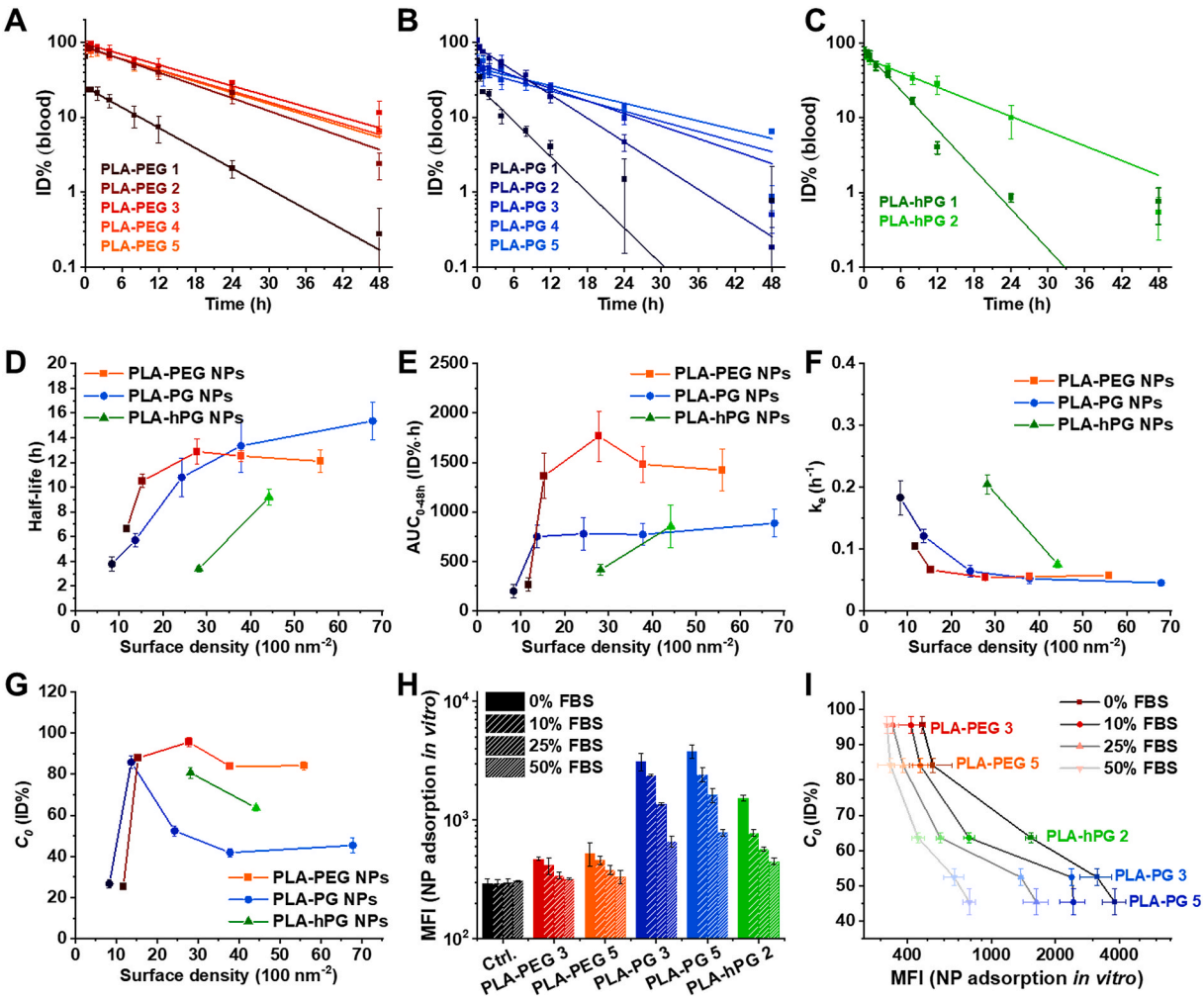

Fig. 2. Pharmacokinetic analysis of PEG-, PG-, and hPG-grafted PLA NPs with various surface densities. Pharmacokinetic profiles of (A) PLA-PEG NPs, (B) PLA-PG NPs, (C) PLA-hPG NPs. (D) Half-life. (E) Area under the concentration-time curve (AUC_{0-48h}). (F) Elimination constant (k_e). (G) Apparent initial concentration (C_0). (H) Mean fluorescence intensity (MFI) of endothelial cells incubated with NPs for 5 min depending on serum concentration. (I) Correlation between fluorescence intensity of NP-adsorbed cells and C_0.

rapid decrease in NP blood concentration immediately after administration might be attributed to the adsorption of PLA-PG NPs to endothelial cells while they are distributing through bloodstream. To test this, we simulated this short-term exposure of NPs with blood endothelial cells *in vitro*. Human umbilical vein endothelial cells (HUVEC) were treated with NPs with dense PEG, PG, or hPG coatings for 5 min at different FBS concentrations and analyzed the cellular association of NP by adsorption by flow cytometry. The cells were incubated with NPs only for a short periods of time, so only adsorption of NPs on cell membranes was measured as other cellular association pathways including phagocytosis or micropinocytosis at this timescale would be minimal. Significant differences in NP adsorption were observed between NPs, with PLA-PG NPs exhibiting an approximately 2 to 5-fold increase in adsorption on HUVEC compared to PLA-PEG NPs (Fig. 2H, in which NP adsorption is plotted on a log-scale). We observed a reduction in NP adsorption with increasing FBS concentration in the treating medium, with PLA-PG NPs and PLA-hPG NPs showing higher adsorption relative to PLA-PEG NPs at every FBS concentration. Notably, C_0 and the adsorption of NPs *in vitro* are clearly correlated, suggesting that the rapid reduction in blood concentration of PLA-PG NPs and PLA-hPG NPs during the distribution phase may be attributed to the adsorption of the NPs on endothelial cells (Fig. 2I).

In addition to 90 nm sized-NPs, we also compared the pharmacokinetics of PLA-PEG NPs and PLA-PG NPs of similar surface density at different sizes (Fig. S10). For small NPs (D_h = 40 nm), PEG and PG-coating only resulted in small differences in pharmacokinetic parameters and circulation profile. However, large-sized NPs (D_h = 150 nm) grafted with PG were more rapidly cleared than PEGylated NPs. Both PLA-PEG-L and PLA-PG-L showed similar clearance profiles and pharmacokinetic parameters as PLA-PEG NP2 and PLA-PG NP2 with similar surface density (~15 per 100 nm^2). The half-life of 150 nm-sized NPs also followed the correlation between the half-life of and surface density of polymer observed in the series of 90 nm-sized NPs (Fig. S12), but 40 nm-sized NPs had a shorter half-life. On the other hand, the smaller nanoparticles exhibited a larger AUC and larger nanoparticles showed a slightly smaller AUC compared to 90 nm-sized NPs having similar density of grafted polymer, regardless of the type of polymer (PEG or PG) grafted on NP surface.

Although PG-grafted NPs exhibited a smaller AUC and C_0 compared to PEG-grafted NPs, their pharmacokinetics and stealth properties were remarkably similar to PEG and superior to other reported PEG-alternatives. In particular, the circulation half-lives and AUC of PLA NPs decorated with PEG-alternatives other than PG were less than half the value of PEGylated NP controls. The AUC of PLA-PVP NPs has been reported as one tenth of that of PLA-PEG NPs; PLA-poly(phosphoester) NPs cleared even more rapidly with less than 2% of the AUC of PLA-PEG [59]. The clearance rates of PLA-PVP, PLA-poly(4-acryloylmorpholine), and PLA-poly(N,*N*-dimethylacrylamide) NPs were also

reported to be at least four times larger than that of PLA-PEG NPs [21].

3.5. Biodistribution

We evaluated the effect of surface density of PEG, PG or hPG on NP biodistribution in mice 48 h after intravenous administration (Fig. 3, Fig. S13). The major elimination process of NPs administered intravenously is via the MPS, which results in accumulation of NPs in liver or spleen [66]. In agreement with prior reports, NPs with a higher PEG surface density showed less accumulation in both liver and spleen with similar trends observed for PG and hPG-grafted NPs [42,50,54]. However, we found distinct differences in biodistribution between PG and PEG-grafted NPs. Accumulation of PLA-PG NPs in both liver and spleen was at a minimum for all densities >10 PG per 100 nm^2, but >25 PEG per 100 nm^2 was needed for PLA-PEG NPs to achieve a similar reduction in accumulation. For NPs with high surface density (>30 chains per 100 nm^2), accumulation in liver and spleen remained constant for both PEG- and PG-grafted NPs. This suggests that PG of the same length as PEG provides sufficient evasion of MPS clearance at a lower surface density compared to PEG, possibly due to higher molecular weight and bulkier repeating unit of PG. Almost no NPs were detected in kidneys and lungs with no significant difference in the accumulation between PEG- and PG-grafted NPs (Fig. S13). Biodistribution of PLA-hPG NP1 was similar to that of PLA-PG NP1. However, PLA-hPG NP2 showed less accumulation in liver and spleen than PLA-PG NP1 but slightly more compared with other PLA-PG NPs.

We additionally compared the biodistribution of PLA-PG and PLA-PEG NPs of different sizes (s and L) to 90 nm NPs of different surface densities (Fig. S14). PLA-PEG-s accumulated less than PLA-PG-s in both liver and spleen, whereas PLA-PEG-L accumulated more than PLA-PG-L, which is consistent with the accumulation of NP2s having similar surface densities. Comparing the small and large NPs with the series of 90 nm-sized NPs, accumulation in the spleen increased as NP size grew, which is commonly found with other nanomaterials (Fig. S15) [50].

3.6. Antibody generation and binding affinity

Anti-PEG antibodies including IgM and immunoglobulin G (IgG) are major factors affecting pharmacokinetics and efficacies of PEGylated therapeutics and NPs by causing ABC [6–8]. To evaluate the anti-PEG antibody responses to grafted polymers on NPs, we intravenously administered NPs to BALB/c mice and analyzed the anti-PEG IgM and IgG levels after 7 days, as it has been reported that the level of anti-PEG IgM in serum reaches a maximum in mice within a week after sensitization [6,67].

First, we quantified the anti-PEG IgM and IgG concentration in serum using an enzyme-linked immunosorbent assay (ELISA). In agreement with prior reports [67], a significant amount of anti-PEG IgM was detected in the serum of mice sensitized with PLA-PEG NPs. PLA-PEG NP3 and PLA-PEG NP5, which contained enough PEG to have prolonged blood circulation, induced similar levels of anti-PEG IgM in mice (Fig. 4A). Notably, we also found significant levels of IgM in mice sensitized with PLA-PG NPs, but not with PLA-hPG. Depending on the injection dose of NPs, anti-PEG IgM responses varied. The doses eliciting maximum anti-PEG IgM generation by PLA-PEG NP and PLA-PG NP were both between 5 $mg{\cdot}kg^{-1}$ and 10 $mg{\cdot}kg^{-1}$ (Fig. S20). The level of anti-PEG IgG was relatively low compared to IgM for all NPs consistent with other reports on the administration of a single dose of PEGylated NPs [8].

To analyze the level of anti-PEG IgM adhesion to our grafted polymers, we performed ELISA with PLA-PEG, PLA-PG, PLA-hPG, or PLA-coated well plates. The coating of well plates with polymer was indirectly verified by the selective binding of anti-PEG IgM standards to a PLA-PEG-coated plate, but not other plates (Fig. S16). To rule out the effect of non-specific binding of IgM to polymer-coated plates, we treated each plate with isotype mice IgM and confirmed that non-specific binding of IgM was not significant at IgM concentrations below 1 $\mu g{\cdot}ml^{-1}$ (Fig. S16). The highest IgM level was observed from the mice sensitized with PLA-PEG NPs, followed by ones administered with PLA-PG NPs (Fig. S4C, Fig. S17). No significant level of IgM was observed on plates coated with PLA-PG (Fig. 4D) or serum from animals sensitized with PLA-hPG (Fig. S4D, Fig. S17).

In addition, we performed competitive binding ELISA using BSA-PEG-coated plates to evaluate cross-reactivity and relative binding affinities of IgM antibodies to PLA-PEG, PLA-PG and PLA-hPG NPs. First, anti-PEG IgM standard was used to evaluate relative cross-reactivity of anti-PEG IgM to PG or PG-grafted NPs. Briefly, anti-PEG IgM was treated with various concentrations of free polymers PEG or PG, as well as PLA-

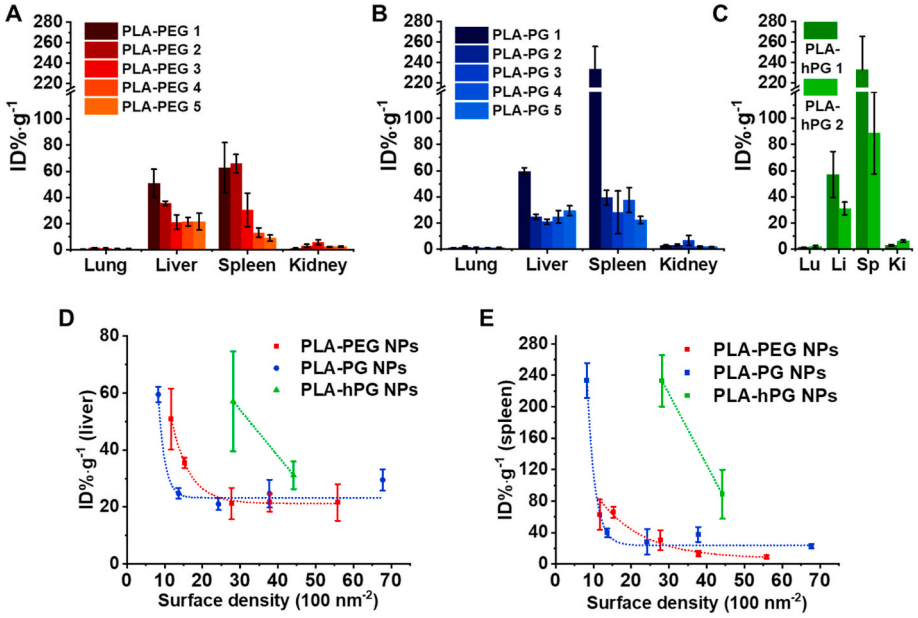

Fig. 3. Biodistribution of PLA-PEG NPs, PLA-PG NPs, and PLA-hPG NPs with various polymer surface densities. (A–C) Accumulation of PLA-PEG NPs, PLA-PG NPs, and PLA-hPG NPs in lung (Lu), liver (Li), spleen (Sp), and kidney (Ki). (D–E) Correlation between accumulation and surface polymer densities in (D) liver and (E) spleen.

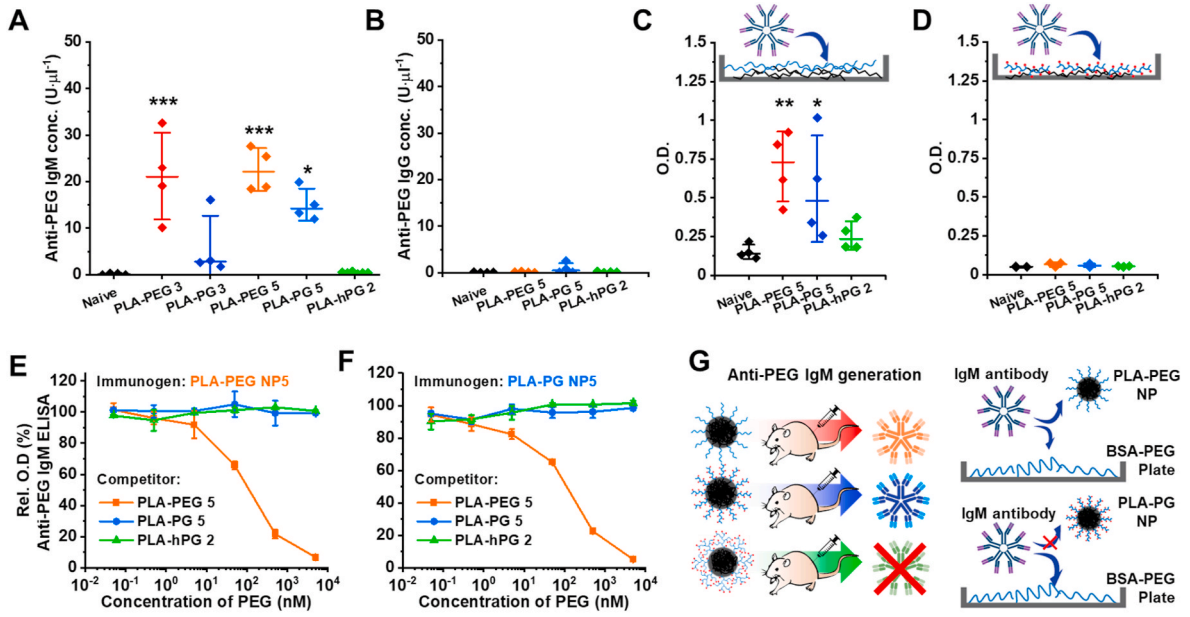

Fig. 4. Antibody responses to PEG-, PG-, and hPG-grafted PLA NPs, and binding affinity. (A) Serum concentration of anti-PEG IgM obtained from mice injected with PEG-, PG-, or hPG-grafted PLA NPs. (B) Serum concentration of anti-PEG IgG concentration from mice. (C–D) IgM antibody in serum from mice detected with PLA-PEG coated well and PLA-PG coated well. (E–F) Competitive binding assay of IgM induced by serum from PLA-PEG NP5 injected mice or serum from PLA-PG NP5 injected mice on PEG-coated plate using various NP competitors (PLA-PEG 5, PLA-PG 5, or PLA-hPG 2). (G) Administration of PLA-PEG NP or PLA-PG NP induced generation of PEG-binding IgM antibodies in mice but PLA-hPG did not (left). Both IgM antibodies induced by PLA-PEG or PLA-PG NPs had higher binding affinity to PLA-PEG NPs than to PLA-PG NPs (right). ($n = 4$, $^*P < 0.05$, $^{**}P < 0.005$, $^{***}P < 0.0005$).

PEG NPs or PLA-PG NPs of two different surface densities on PEG-coated plates, and the percentage of attached IgM on the plate was obtained by performing ELISA analysis (Fig. S18). Both PEGylated NPs tested showed an equivalent level of interference, suggesting the relative affinities of anti-PEG IgM to PEGylated NPs were not affected by the PEG surface density but by molar concentration of PEG. Free methoxy-PEG did not interfere with binding of anti-PEG IgM to the BSA-PEG plate, in agreement with a previous report [67]. Interestingly, anti-PEG IgM also did not show observable binding to PLA-PG NPs or PG at any concentration. Anti-PEG IgM did not bind to the PLA-PG-coated plate (Fig. S16A); therefore, competitive binding assays confirmed that the cross-reactivity of anti-PEG IgM with PLA-PG NPs is negligible.

The same competitive binding assay was conducted using the sera of mice sensitized with PLA-PEG NPs or PLA-PG NPs containing significantly high levels of anti-PEG IgM (Fig. 4E and F). IgM generated by sensitization of mice to PLA-PEG NPs had a comparable relative binding affinity to PLA-PEG NPs as anti-PEG IgM standard over PEG-coated plates (Fig. S19), but no measurable affinity to PLA-PG NPs and PLA-hPG NPs. In summary, PLA-PEG and PLA-PG NPs elicited anti-PEG responses, but PLA-hPG did not; anti-PEG IgM did not show binding affinity to PLA-PG or PLA-hPG NPs (Fig. 4G). Experiments using various polymer-coated plates demonstrated that a significant level of IgM binding to PG or hPG was not detected from the serum of mice sensitized with PLA-PG or PLA-hPG NPs. As binding affinities of PLA-PG and PLA-hPG to anti-PEG IgM were remarkably small, regardless of the immunogen inoculated, we anticipate negligible ABC effect upon multiple administrations.

3.7. Accelerated blood clearance

To evaluate the effect of anti-PEG antibodies *in vivo*, ABC was studied by re-administration of the same NPs 7 days after sensitization of mice with NPs (Fig. 5). Since the generation of anti-PEG IgM starts to decrease at the dose of 20 mg·kg^{-1} (Fig. S20), which has been used for pharmacokinetic analysis, the ABC effect was evaluated with 10 mg·kg^{-1}. A significant reduction in both blood half-life and AUC was observed for PLA-PEG NPs after the second administration (Fig. 5A–C). Specifically, the AUC of PLA-PEG NP3 and PLA-PEG NP5 decreased by a factor of 3.7 and 2.3 respectively when compared to the same NPs administered to naïve control mice (Fig. 5B and C). The ABC effect of PLA-PEG NP3 was more pronounced than for PLA-PEG NP5, although the IgM level in serum was similar for both groups (Fig. 4A). In contrast, neither PLA-PG NPs nor PLA-hPG NP exhibited ABC effects, regardless of surface density; their pharmacokinetic parameters were maintained despite sensitization at the dose of 10 mg·kg^{-1}. Comparing pharmacokinetics between PEG and PG grafted NPs, both half-life and AUC of PLA-PEG NPs were significantly superior to that of PLA-PG or PLA-hPG NPs at the initial administration. Their pharmacokinetic parameters were improved compared to PLA-PEG NP3, but were similar to that of PLA-PEG NP5, even though the PG and hPG grafted NPs did not show an ABC effect after second administration.

Considering that PEG-specific IgM was generated by PLA-PG NPs, it is evident that PLA-PG NPs elicited immune responses. Even though we did not observe anti-PG IgM on PLA-PG-coated plates and the IgM generated by PLA-PG NPs had a much stronger binding affinity to PEG rather than PG, we hypothesized that the IgM will still bind to PLA-PG NPs. Thus, we evaluated the ABC effect of PLA-PG NPs by lowering the dose administered (1 and 5 mg·kg^{-1}). A slight but significant reduction of AUC could be observed at the 5 mg·kg^{-1} dose, and the reduction appeared to be larger by reducing the dose to 1 mg·kg^{-1} (Fig. S25). However, ABC effects were still smaller compared to PLA-PEG NPs, and the terminal half-lives ($t_{1/2}$) of PLA-PG NPs were consistent at both doses. Similar to the 10 mg·kg^{-1} dose, PLA-PG NPs cleared relatively faster than PLA-PEG NPs at the first administration with doses of 1 and 5 mg·kg^{-1}, but both half-life and AUC of sensitized mice appeared to be superior at the dose of 1 mg·kg^{-1}.

The ABC effects are attributed to binding of antibodies to drugs or NPs, causing faster elimination in blood; therefore, it is expected that the change in pharmacokinetic parameters of PEGylated NPs by the ABC effect should depend on the ratio of anti-PEG IgM to NPs [10,68]. Specifically, a stronger ABC effect of PEGylated NPs is observed when the antibody to NP ratio is higher, whereas no significant change in

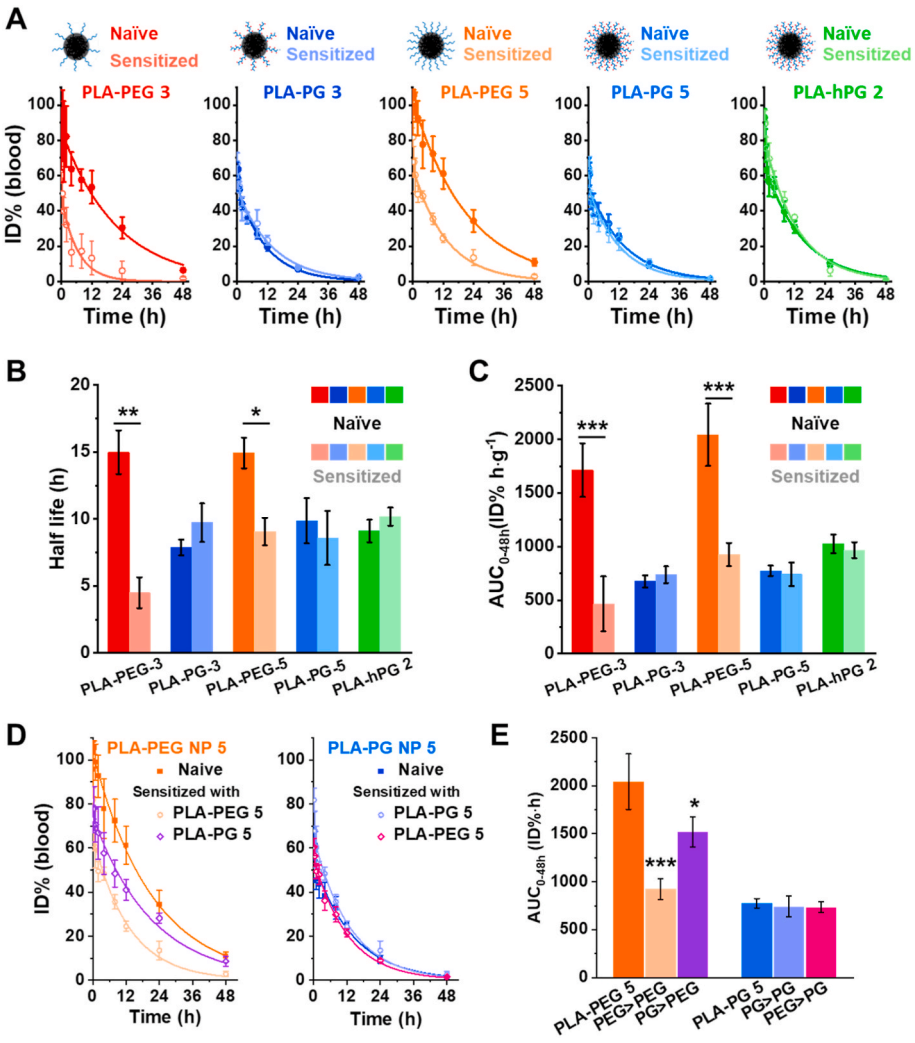

Fig. 5. Evaluation of accelerated blood clearance (ABC) of PEG-, PG-, and hPG-grafted PLA NPs. (A) Pharmacokinetic profiles of NPs, as percent dose per gram of blood over time and their first-order exponential decay curves. (B–C) Changes in pharmacokinetic parameters terminal half-life ($t_{1/2}$) and area under the concentration time curve ($AUC_{0-48\ h}$) before and after NP-sensitization. (D–E) Evaluation of ABC effect analyzing cross-reactivity of antibodies induced by PLA-PEG or PLA-PG NPs. Pharmacokinetic profiles of PLA-PEG NP5 and PLA-PG NP5 in naïve and sensitized mice with PLA-PEG or PLA-PG NP and area under the concentration time curve ($AUC_{0-48\ h}$). ($n = 4$, $^{*}P < 0.05$, $^{**}P < 0.005$, $^{***}P < 0.0005$).

pharmacokinetic parameters occurs if an excess of NPs is administered even with a similar level of anti-PEG IgM in blood serum [69]. Our results on ABC due to PLA-PEG NP3 and NP5 obey this relationship. Despite similar levels of IgM antibody and NP dose, the concentration of PLA-PEG NP5 administered was higher than that of PLA-PEG NP3, resulting in a weaker ABC effect for PLA-PEG NP5 than PLA-PEG NP3 (Table S5). Notably, no significant ABC effect was observed for PLA-PG NP5 at a dose of 10 mg·kg^{-1}, even though the ratio of anti-PEG IgM antibody to NP administered was enough to result in a significant ABC effect for PLA-PEG NPs (Table S5). However, at lower doses where the ratio of antibody to NP was much larger, PLA-PG NP5 exhibited ABC effects. These findings suggest that the impact of the serum anti-PEG IgM on the ABC effect of PLA-PG NPs is much smaller due to the low binding affinity of IgM to PLA-PG NPs.

To study the cross-reactivities *in vivo*, we also evaluated the ABC effects of PLA-PG NP5 in mice sensitized with PLA-PEG NP5 at a dose of 10 mg·kg^{-1}, and vice versa (Fig. 5D). As a lower concentration of anti-PEG IgM was detected in mice sensitized with PLA-PEG NP5 than with PLA-PG NP5 (Fig. 4A), a weaker ABC effect of PLA-PEG NP5 was expected with mice sensitized with PLA-PG NP5. In fact, a significant but slightly weaker ABC effect was observed for PLA-PEG NPs in mice sensitized with PLA-PG NPs (Fig. 5D and E, and Table S5). The pharmacokinetic profile of PLA-PG NPs was maintained in mice sensitized with PLA-PEG NP.

3.8. Discussion of anti-PEG/PG responses and cross-reactivity

Adaptive immunity against polymers such as PEG is governed by various factors [10]. For example, it is known that the immunogenicity of polymers strongly depends on the immunogenicity of conjugated therapeutics, the structure or end-groups of the polymer, and the hydrophobicity of conjugated molecules [10,70]. In contrast to protein-PEG conjugates, anti-PEG immune responses elicited by NPs appear to be generated by the thymus independent (TI-2) pathway in which helper T-cells are not involved [10]. PLA-PEG NPs and PLA-PG NPs are likely to activate this same TI-2 pathway, triggering various B-cells to specifically interact with PEG and PG chains to produce anti-polymer IgM. Bell-shaped dose responses on antibody induction—with strong antibody responses at intermediate dose (Fig. S20), and weak IgG induction (Fig. 4B)—support the claim that our biodegradable polymeric NPs induce immune responses via the TI-2 pathway.

We did not observe anti-PG IgM using polymer-coated ELISA plates (Fig. 4E and Fig. S22). In addition, PLA-PG NPs did not exhibit an ABC effect at a high dose of 10 mg·kg^{-1} (Fig. 5), whereas an ABC effect was observed at low doses (Fig. S25). The competitive ELISA and evaluation of cross-reactivity of IgM by ABC effect suggest that IgM produced by PLA-PG NPs shows higher binding affinity to PLA-PEG NPs than PLA-PG NPs. These observations suggest either that the PG-grafted NP generates an anti-PEG IgM response or that anti-PG IgM has strong cross-reactivity to PEGylated NPs.

Any cross-reactivity of anti-PG IgM to PEG NPs is likely related to the

structural similarity of PG to PEG (Fig. 1A). The cross-reactivity of anti-PEG antibodies to other polymers has been studied, showing that some monoclonal antibodies as well as anti-PEG antibodies isolated from human samples have significant binding affinities to polymers with the C–C–O backbone, such as polypropylene glycol and polytetramethylene ether, but not to polybutylene adipate, polyethyleneimine, and dextran [71]. Moreover, it is known that the methoxy terminal group plays a crucial role in both induction and binding of anti-PEG antibodies [72,73]. For example, methoxy-PEG has been observed to induce higher antibody responses in both protein-conjugates and PEGylated liposomes than hydroxyl-PEG. Linear PG in this study also has a methoxy end group introduced by the methoxyethanol initiator and a linear ethylene-oxide backbone like methoxy-PEG. However, hPG has less structural similarity to methoxy-PEG due to the use of AB_2-type monomer creating two different linear units (2 or 3 carbon) in the backbone apart from its hyperbranched structure, despite having glycerol as repeating units like linear PG. In addition, the outer surface of hPG is terminated with vicinal diols [30,74] (Fig. S26).

Nonetheless, the low binding affinity of anti-PEG IgM to PLA-PG NPs, which has been verified by both ELISA binding and an ABC effect, may also be attributed to structural differences. It has been demonstrated that polymers need at least three ethylene glycol (EG) repeating units to be selectively bound with anti-PEG antibodies [75], and the binding affinity of EG oligomer is dramatically reduced as EG chains get shorter [76]. Moreover, from structural analysis, the selectivity of anti-PEG antibodies is attributed to the insertion process of PEG chains in the open ring structure at the anti-PEG antibody binding site and stabilization of PEG backbone chain to binding site via van der Waals interactions along the ring paratope surface [77]. Thus, it can be suggested that the terminal EG oligomer on linear PG is too short to serve as an epitope for the binding of antibodies as compared to PEG. In addition, the hydroxyl groups on the PG backbone seem to inhibit the binding process of anti-PEG antibodies resulting in low binding affinity.

The induction of antibody production by B-cells and the neutralization of the immunogen by released antibodies are based on the immunoglobulins having the same binding sites. However, the flexibility of PEG, which does not have a fixed conformation, makes it difficult to elucidate the immunogenicity and specific binding of PEG and alternative polymers. In this work, we observed anti-PEG antibody responses generated by the structurally similar linear PG, but further research is needed to fully explain the relationship between the cross-reactive immune responses and structural similarities of polymers. Since it is known that anti-polymer responses can be induced by highly immunogenic protein-polymer conjugates [70], additional studies on the anti-polymer responses of PG- and hPG-protein conjugates could help to clarify this phenomenon.

4. Conclusions

The concerns about the immune response elicited by PEGylated therapeutics and vaccines, particularly when multi-dose administration is necessary, warrant the development of PEG-alternative polymers. Although polyglycerol (PG), which has the same ethylene oxide backbone as PEG, is a promising alternative for the stealth coating of nanocarriers, the structural impact of PG-grafting on pharmacokinetics and immunogenicity has not been extensively studied. In this work, we synthesized linear PG with an analogous length and end-group composition as widely used mPEG, prepared a library of NPs with PLA core having various surface densities of PEG, linear-PG, or branched-PG, and evaluated the performance of PG grafting in terms of pharmacokinetics and immunogenicity.

Grafting PG on polymeric NPs resulted in enhanced blood half-life but smaller AUC compared to PEGylated NPs, likely due to the adsorption of NPs to endothelial cells. However, PG provided sufficient surface coverage for exhibiting a stealth-effect at a lower surface density compared to PEG, as indicated by the reduced accumulation in liver and spleen. We also observed that the composition of the protein layer adsorbed on the NP surface was different between PLA-PG and PLA-PEG NPs when the PG or PEG surface density was low, but became almost identical at higher PG or PEG surface density. For hPG-grafted NPs, the less flexible and heterogenous structure of the branched polymer may have an impact on the assembly of NPs as indicated by their lower exposure ratio in the hPG corona than linear polymers, and the observation of more complement proteins and immunoglobulins on the NP surface. However, with sufficient hPG density on the NP surface, pharmacokinetic parameters and biodistribution approached the results of linear-PG grafted NPs. Notably, we found that linear PG-grafted NPs induced the generation of IgM that bind to PEG in mice, while having minimal binding to either PG or hPG. In contrast, hPG-grafted NPs did not elicit significant anti-PEG IgM responses. Supported by pharmacokinetic analysis *in vivo*, both PG- and hPG-grafted NPs dramatically reduced ABC effects, even at low doses with significant levels of anti-PEG antibody.

The surface identity of NPs, which is determined by the type and molecular weight of the stealth polymer as well as its surface density, is a key factor that modulates the behavior of therapeutic NPs in various physiological environments [43,45,46]. This behavior is observed in NP pharmacokinetics, biodistribution, cellular internalization, and efficacy of therapeutic molecules. As more PEGylated nanocarriers, including the COVID-19 mRNA vaccine [78,79], are approved for use in humans, the concern for their immunogenicity is growing [80]. Therefore, it is becoming more crucial to develop alternative polymers for NP coating and to study their immunogenicity. Our findings on the impact of structural differences of grafted polymers on pharmacokinetics and immunogenicity provide insight into designs for surface-grafted polymers that can overcome the immunogenicity of PEG while maintaining appropriate stealth properties.

Declaration of competing interest

The authors declare that they have no known competing financial interests or personal relationships that could have appeared to influence the work reported in this paper.

Credit author statement

K. Shin: Conceptualization, Methodology, Formal analysis, Investigation, Writing – original draft, Writing – review & editing, Visualization; H.-W. Suh: Investigation, Writing – review & editing; J. Grundler: Investigation, Writing–review & editing; A. Y. Lynn: Investigation, Writing – review & editing; J. U. Pothupitiya: Investigation; Z. M. Moscato: Investigation; M. Reschke: Investigation; L. G. Bracaglia: Methodology; A. S. Piotrowski-Daspit: Methodology, Writing–review & editing; W. M. Saltzman: Conceptualization, Supervision, Writing – review & editing, Funding acquisition.

Data availability

The raw/processed data required to reproduce these findings cannot be shared at this time as the data also forms part of an ongoing study.

Acknowledgments

This work was supported by grants from the National Institutes of Health (NIH; EB000487, HL139756, and U01 AI145965) and the Cystic Fibrosis Foundation (CFF; EGAN19XX0). L.G.B. was supported by an NIH-National Research Service Award (NRSA) training grant (T32 DK007276) and a K99/R00 Pathway to Independence award (K99 HL157552). A.S.P. was supported by a K99/R00 Pathway to Independence Award from the NIH (K99 HL151806), as well as a postdoctoral research fellowship award from the CFF (PIOTRO20F0), and a Postdoc-to-Faculty Transition Award from the CFF (PIOTRO21F5). We thank

Gwendolyn Davis-Arrington for assistance with endothelial cell isolation. The mass spectrometers at the Keck MS & Proteomics Resource at Yale University were funded in part by the Yale School of Medicine and by the Office of the Director, NIH (S10OD02365101A1, S10OD019967, and S10OD018034).

Appendix A. Supplementary data

Supplementary data to this article can be found online at https://doi.org/10.1016/j.biomaterials.2022.121676.

References

[1] J.M. Harris, R.B. Chess, Effect of pegylation on pharmaceuticals, Nat. Rev. Drug Discov. 2 (2003) 214–221, https://doi.org/10.1038/nrd1033.
[2] J. Zheng, L. Li, H.-K. Tsao, Y.-J. Sheng, S. Chen, S. Jiang, Strong repulsive forces between protein and oligo (ethylene glycol) self-assembled monolayers: a molecular simulation study, Biophys. J. 89 (2005) 158–166, https://doi.org/10.1529/biophysj.105.059428.
[3] S.R. Meyers, M.W. Grinstaff, Biocompatible and bioactive surface modifications for prolonged in vivo efficacy, Chem. Rev. 112 (2012) 1615–1632, https://doi.org/10.1021/cr2000916.
[4] J.T. Huckaby, S.K. Lai, PEGylation for enhancing nanoparticle diffusion in mucus, Adv. Drug Deliv. Rev. 124 (2018) 125–139, https://doi.org/10.1016/j.addr.2017.08.010.
[5] J.V. Jokerst, T. Lobovkina, R.N. Zare, S.S. Gambhir, Nanoparticle PEGylation for imaging and therapy, Nanomedicine 6 (2011) 715–728, https://doi.org/10.2217/nnm.11.19.
[6] M. Ichihara, T. Shimizu, A. Imoto, Y. Hashiguchi, Y. Uehara, T. Ishida, H. Kiwada, Anti-PEG IgM response against PEGylated liposomes in mice and rats, Pharmaceutics 3 (2010) 1–11, https://doi.org/10.3390/pharmaceutics3010001.
[7] Y. Mima, Y. Hashimoto, T. Shimizu, H. Kiwada, T. Ishida, Anti-PEG IgM is a major contributor to the accelerated blood clearance of polyethylene glycol-conjugated protein, Mol. Pharm. 12 (2015) 2429–2435, https://doi.org/10.1021/acs.molpharmaceut.5b00144.
[8] G.T. Kozma, T. Mészáros, I. Vashegyi, T. Fülöp, E. Örfi, L. Dézsi, L. Rosivall, Y. Bavli, R. Urbanics, T.E. Mollnes, Y. Barenholz, J. Szebeni, Pseudo-anaphylaxis to polyethylene glycol (PEG)-Coated liposomes: roles of anti-PEG IgM and complement activation in a porcine model of human infusion reactions, ACS Nano 13 (2019) 9315–9324, https://doi.org/10.1021/acsnano.9b03942.
[9] T. Ishihara, M. Takeda, H. Sakamoto, A. Kimoto, C. Kobayashi, N. Takasaki, K. Yuki, K.-i. Tanaka, M. Takenaga, R. Igarashi, T. Maeda, N. Yamakawa, Y. Okamoto, M. Otsuka, T. Ishida, H. Kiwada, Y. Mizushima, T. Mizushima, Accelerated blood clearance phenomenon upon repeated injection of PEG-modified PLA-nanoparticles, Pharm. Res. (N. Y.) 26 (2009) 2270–2279, https://doi.org/10.1007/s11095-009-9943-x.
[10] B.M. Chen, T.L. Cheng, S.R. Roffler, Polyethylene glycol immunogenicity: theoretical, clinical, and practical aspects of anti-polyethylene glycol antibodies, ACS Nano 15 (2021) 14022–14048, https://doi.org/10.1021/acsnano.1c05922.
[11] Q. Yang, T.M. Jacobs, J.D. McCallen, D.T. Moore, J.T. Huckaby, J.N. Edelstein, S. K. Lai, Analysis of pre-existing IgG and IgM antibodies against polyethylene glycol (PEG) in the general population, Anal. Chem. 88 (2016) 11804–11812, https://doi.org/10.1021/acs.analchem.6b03437.
[12] B.-M. Chen, Y.-C. Su, C.-J. Chang, P.-A. Burnouf, K.-H. Chuang, C.-H. Chen, T.-L. Cheng, Y.-T. Chen, J.-Y. Wu, S.R. Roffler, Measurement of pre-existing IgG and IgM antibodies against polyethylene glycol in healthy individuals, Anal. Chem. 88 (2016) 10661–10666, https://doi.org/10.1021/acs.analchem.6b03109.
[13] I. Ekladious, Y.L. Colson, M.W. Grinstaff, Polymer–drug conjugate therapeutics: advances, insights and prospects, Nat. Rev. Drug Discov. 18 (2019) 273–294, https://doi.org/10.1038/s41573-018-0005-0.
[14] P. Zhang, F. Sun, S. Liu, S. Jiang, Anti-PEG antibodies in the clinic: current issues and beyond PEGylation, J. Contr. Release 244 (2016) 184–193, https://doi.org/10.1016/j.jconrel.2016.06.040.
[15] Y.-C. Hsieh, H.-E. Wang, W.-W. Lin, S.R. Roffler, T.-C. Cheng, Y.-C. Su, J.-J. Li, C.-C. Chen, C.-H. Huang, B.-M. Chen, J.-Y. Wang, T.-L. Cheng, F.-M. Chen, Pre-existing anti-polyethylene glycol antibody reduces the therapeutic efficacy and pharmacokinetics of PEGylated liposomes, Theranostics 8 (2018) 3164–3175, https://doi.org/10.7150/thno.22164.
[16] A. Moreno, G.A. Pitoc, N.J. Ganson, J.M. Layzer, M.S. Hershfield, A.F. Tarantal, B. A. Sullenger, Anti-PEG antibodies inhibit the anticoagulant activity of PEGylated aptamers, Cell Chem. Biol. 26 (2019) 634–644, https://doi.org/10.1016/j.chembiol.2019.02.001.
[17] T.J. Povsic, M.G. Lawrence, A.M. Lincoff, R. Mehran, C.P. Rusconi, S. L. Zelenkofske, Z. Huang, J. Sailstad, P.W. Armstrong, P.G. Steg, C. Bode, R. C. Becker, J.H. Alexander, N.F. Adkinson, A.I. Levinson, R.-P. Investigators, Pre-existing anti-PEG antibodies are associated with severe immediate allergic reactions to pegnivacogin, a PEGylated aptamer, J. Allergy Clin. Immunol. 138 (2016) 1712–1715, https://doi.org/10.1016/j.jaci.2016.04.058.
[18] G. Kozma, T. Shimizu, T. Ishida, J. Szebeni, Anti-PEG antibodies: properties, formation and role in adverse immune reactions to PEGylated nano-biopharmaceuticals, Adv. Drug Deliv. Rev. 154–155 (2020) 163–175, https://doi.org/10.1016/j.addr.2020.07.024.
[19] T.T.H. Thi, E.H. Pilkington, D.H. Nguyen, J.S. Lee, K.D. Park, N.P. Truong, The importance of poly(ethylene glycol) alternatives for overcoming PEG immunogenicity in drug delivery and bioconjugation, Polymers 12 (2020) 298, https://doi.org/10.3390/polym12020298.
[20] G.v. Gaucher, K. Asahina, J. Wang, J.-C. Leroux, Effect of poly(N -vinyl-pyrrolidone)- block -poly(D,L-lactide) as coating agent on the opsonization, phagocytosis, and pharmacokinetics of biodegradable nanoparticles, Biomacromolecules 10 (2009) 408–416, https://doi.org/10.1021/bm801178f.
[21] T. Ishihara, T. Maeda, H. Sakamoto, N. Takasaki, M. Shigyo, T. Ishida, H. Kiwada, Y. Mizushima, T. Mizushima, Evasion of the accelerated blood clearance phenomenon by coating of nanoparticles with various hydrophilic polymers, Biomacromolecules 11 (2010) 2700–2706, https://doi.org/10.1021/bm100754e.
[22] H. Bludau, A.E. Czapar, A.S. Pitek, S. Shukla, R. Jordan, N.F. Steinmetz, POxylation as an alternative stealth coating for biomedical applications, Eur. Polym. J. 88 (2017) 679–688, https://doi.org/10.1016/j.eurpolymj.2016.10.041.
[23] T. Steinbach, F.R. Wurm, Poly(phosphoester)s: a new platform for degradable polymers, Angew. Chem. Int. Ed. 54 (2015) 6098–6108, https://doi.org/10.1002/anie.201500147.
[24] S. Jiang, Z. Cao, Ultralow-fouling, functionalizable, and hydrolyzable zwitterionic materials and their derivatives for biological applications, Adv. Mater. 22 (2010) 920–932, https://doi.org/10.1002/adma.200901407.
[25] M. Debayle, E. Balloul, F. Dembele, X. Xu, M. Hanafi, F. Ribot, C. Monzel, M. Coppey, A. Fragola, M. Dahan, T. Pons, N. Lequeux, Zwitterionic polymer ligands: an ideal surface coating to totally suppress protein-nanoparticle corona formation? Biomaterials 219 (2019), 119357 https://doi.org/10.1016/j.biomaterials.2019.119357.
[26] S.Y. Fam, C.F. Chee, C.Y. Yong, K.L. Ho, A.R. Mariatulqabtiah, W.S. Tan, Stealth coating of nanoparticles in drug-delivery systems, Nanomaterials 10 (2020) 787, https://doi.org/10.3390/nano10040787.
[27] S. Lowe, N.M. O'Brien-Simpson, L.A. Connal, Antibiofouling polymer interfaces: poly(ethylene glycol) and other promising candidates, Polym. Chem. 6 (2014) 198–212, https://doi.org/10.1039/c4py01356e.
[28] A. Thomas, S.S. Müller, H. Frey, Beyond poly(ethylene glycol): linear polyglycerol as a multifunctional polyether for biomedical and pharmaceutical applications, Biomacromolecules 15 (2014) 1935–1954, https://doi.org/10.1021/bm5002608.
[29] S. Abbina, S. Vappala, P. Kumar, E.M.J. Siren, C.C. La, U. Abbasi, D.E. Brooks, J. N. Kizhakkedathu, Hyperbranched polyglycerols: recent advances in synthesis, biocompatibility and biomedical applications, J. Mater. Chem. B 5 (2017) 9249–9277, https://doi.org/10.1039/c7tb02515g.
[30] Y. Deng, J.K. Saucier-Sawyer, C.J. Hoimes, J. Zhang, Y.-E. Seo, J.W. Andrejecsk, W. M. Saltzman, The effect of hyperbranched polyglycerol coatings on drug delivery using degradable polymer nanoparticles, Biomaterials 35 (2014) 6595–6602, https://doi.org/10.1016/j.biomaterials.2014.04.038.
[31] K. Wagener, M. Worm, S. Pektor, M. Schinnerer, R. Thiermann, M. Miederer, H. Frey, F. Rösch, Comparison of linear and hyperbranched polyether lipids for liposome shielding by 18F-radiolabeling and positron emission tomography, Biomacromolecules (2018) 2506–2516, https://doi.org/10.1021/acs.biomac.8b00115.
[32] Y. Zou, S. Ito, F. Yoshino, Y. Suzuki, L. Zhao, N. Komatsu, Polyglycerol grafting shields nanoparticles from protein corona formation to avoid macrophage uptake, ACS Nano 14 (2020) 7216–7226, https://doi.org/10.1021/acsnano.0c02289.
[33] D. Wilms, S.-E. Stiriba, H. Frey, Hyperbranched Polyglycerols, From the controlled synthesis of biocompatible polyether polyols to multipurpose applications, Acc. Chem. Res. 43 (2010) 129–141, https://doi.org/10.1021/ar900158p.
[34] T.H.L. Kim, J.H. Yu, H. Jun, M.Y. Yang, M.-J. Yang, J.-W. Cho, J.W. Kim, J.S. Kim, Y.S. Nam, Polyglycerolated nanocarriers with increased ligand multivalency for enhanced in vivo therapeutic efficacy of paclitaxel, Biomaterials 145 (2017) 223–232, https://doi.org/10.1016/j.biomaterials.2017.08.042.
[35] J.K. Hu, H.-W. Suh, M. Qureshi, J.M. Lewis, S. Yaqoob, Z.M. Moscato, S. Griff, A. K. Lee, E.S. Yin, W.M. Saltzman, M. Girardi, Nonsurgical treatment of skin cancer with local delivery of bioadhesive nanoparticles, Proc. Natl. Acad. Sci. U.S.A. 118 (2021), e2020575118, https://doi.org/10.1073/pnas.2020575118.
[36] Y. Deng, F. Yang, E. Cocco, E. Song, J. Zhang, J. Cui, M. Mohideen, S. Bellone, A. D. Santin, W.M. Saltzman, Improved i.p. drug delivery with bioadhesive nanoparticles, Proc. Natl. Acad. Sci. U.S.A. 113 (2016) 11453–11458, https://doi.org/10.1073/pnas.1523141113.
[37] Y. Deng, A. Ediriwickrema, F. Yang, J. Lewis, M. Girardi, W.M. Saltzman, A sunblock based on bioadhesive nanoparticles, Nat. Mater. 14 (2015) 1278–1285, https://doi.org/10.1038/nmat4422.
[38] C. Schubert, M. Schömer, M. Steube, S. Decker, C. Friedrich, H. Frey, Systematic variation of the degree of branching (DB) of polyglycerol via oxyanionic copolymerization of glycidol with a protected glycidyl ether and its impact on rheological properties, Macromol. Chem. Phys. 219 (2018), 1700376, https://doi.org/10.1002/macp.201700376.
[39] M.I. ul-haq, B.F.L. Lai, R. Chapanian, J.N. Kizhakkedathu, Influence of architecture of high molecular weight linear and branched polyglycerols on their biocompatibility and biodistribution, Biomaterials 33 (2012) 9135–9147, https://doi.org/10.1016/j.biomaterials.2012.09.007.
[40] A.S.A. Lila, Y. Uehara, T. Ishida, H. Kiwada, Application of polyglycerol coating to plasmid DNA lipoplex for the evasion of the accelerated blood clearance phenomenon in nucleic acid delivery, J. Pharmacol. Sci. (2014) 557–566, https://doi.org/10.1002/jps.23823.
[41] A.S.A. Lila, K. Nawata, T. Shimizu, T. Ishida, H. Kiwada, Use of polyglycerol (PG), instead of polyethylene glycol (PEG), prevents induction of the accelerated blood clearance phenomenon against long-circulating liposomes upon repeated

administration, Int. J. Pharm. (2013) 235–242, https://doi.org/10.1016/j.ijpharm.2013.07.059.
[42] N. Bertrand, P. Grenier, M. Mahmoudi, E.M. Lima, E.A. Appel, F. Dormont, J. M. Lim, R. Karnik, R. Langer, O.C. Farokhzad, Mechanistic understanding of in vivo protein corona formation on polymeric nanoparticles and impact on pharmacokinetics, Nat. Commun. 8 (2017) 777, https://doi.org/10.1038/s41467-017-00600-w.
[43] S. Zhang, H. Gao, G. Bao, Physical principles of nanoparticle cellular endocytosis, ACS Nano 9 (2015) 8655–8671, https://doi.org/10.1021/acsnano.5b03184.
[44] J.-L. Wang, X.-J. Du, J.-X. Yang, S. Shen, H.-J. Li, Y.-L. Luo, S. Iqbal, C.-F. Xu, X.-D. Ye, J. Cao, J. Wang, The effect of surface poly(ethylene glycol) length on in vivo drug delivery behaviors of polymeric nanoparticles, Biomaterials 182 (2018) 104–113, https://doi.org/10.1016/j.biomaterials.2018.08.022.
[45] A.E. Nel, L. Mädler, D. Velegol, T. Xia, E.M.V. Hoek, P. Somasundaran, F. Klaessig, V. Castranova, M. Thompson, Understanding biophysicochemical interactions at the nano–bio interface, Nat. Mater. 8 (2009) 543–557, https://doi.org/10.1038/nmat2442.
[46] S.M. Moghimi, A.C. Hunter, T.L. Andresen, Factors controlling nanoparticle pharmacokinetics: an integrated analysis and perspective, Annu. Rev. Pharmacol. Toxicol. 52 (2012) 481–503, https://doi.org/10.1146/annurev-pharmtox-010611-134623.
[47] A.C. Anselmo, S. Mitragotri, Nanoparticles in the clinic: an update, Bioeng. Transl. Med. 4 (2019), e10143, https://doi.org/10.1002/btm2.10143.
[48] L.G. Bracaglia, A.S. Piotrowski-Daspit, C.-Y. Lin, Z.M. Moscato, Y. Wang, G. T. Tietjen, W.M. Saltzman, High-throughput quantitative microscopy-based half-life measurements of intravenously injected agents, Proc. Natl. Acad. Sci. U.S.A. 117 (2020) 3502–3508, https://doi.org/10.1073/pnas.1915450117.
[49] J. Hrkach, D.V. Hoff, M.M. Ali, E. Andrianova, J. Auer, T. Campbell, D.D. Witt, M. Figa, M. Figueiredo, A. Horhota, S. Low, K. McDonnell, E. Peeke, B. Retnarajan, A. Sabnis, E. Schnipper, J.J. Song, Y.H. Song, J. Summa, D. Tompsett, G. Troiano, T.V.G. Hoven, J. Wright, P. LoRusso, P.W. Kantoff, N.H. Bander, C. Sweeney, O. C. Farokhzad, R. Langer, S. Zale, Preclinical development and clinical translation of a PSMA-targeted docetaxel nanoparticle with a differentiated pharmacological profile, Sci. Transl. Med. 4 (2012), https://doi.org/10.1126/scitranslmed.3003651, 128ra139.
[50] N. Hoshyar, S. Gray, H. Han, G. Bao, The effect of nanoparticle size on in vivo pharmacokinetics and cellular interaction, Nanomedicine 11 (2016) 673–692, https://doi.org/10.2217/nnm.16.5.
[51] F. Wurm, J. Nieberle, H. Frey, Double-hydrophilic linear-hyperbranched block copolymers based on poly(ethylene oxide) and poly(glycerol), Macromolecules 41 (2008) 1184–1188, https://doi.org/10.1021/ma702308g.
[52] M. Kuhlmann, J. Groll, Dispersity control of linear poly(glycidyl ether)s by slow monomer addition, RSC Adv. 5 (2015) 67323–67326, https://doi.org/10.1039/c5ra08067c.
[53] S. Sosnowski, Selective cleavage of acetal bonds in copolymers with polylactide block, J. Polym. Sci. Polym. Chem. 46 (2008) 6978–6982, https://doi.org/10.1002/pola.22993.
[54] X.-J. Du, J.-L. Wang, W.-W. Liu, J.-X. Yang, C.-Y. Sun, R. Sun, H.-J. Li, S. Shen, Y.-L. Luo, X.-D. Ye, Y.-H. Zhu, X.-Z. Yang, J. Wang, Regulating the surface poly (ethylene glycol) density of polymeric nanoparticles and evaluating its role in drug delivery in vivo, Biomaterials 69 (2015) 1–11, https://doi.org/10.1016/j.biomaterials.2015.07.048.
[55] J.S. Hrkach, M.T. Peracchia, A. Bomb, n. Lotan, R. Langer, Nanotechnology for biomaterials engineering: structural characterization of amphiphilic polymeric nanoparticles by 1H NMR spectroscopy, Biomaterials 18 (1997) 27–30, https://doi.org/10.1016/S0142-9612(96)00077-4.
[56] F. Brandl, N. Bertrand, E.M. Lima, R. Langer, Nanoparticles with photoinduced precipitation for the extraction of pollutants from water and soil, Nat. Commun. 6 (2015) 7765, https://doi.org/10.1038/ncomms8765.
[57] D.E. Owens, N.A. Peppas, Opsonization, biodistribution, and pharmacokinetics of polymeric nanoparticles, Int. J. Pharm. 307 (2006) 93–102, https://doi.org/10.1016/j.ijpharm.2005.10.010.
[58] C.D. Walkey, J.B. Olsen, H. Guo, A. Emili, W.C. Chan, Nanoparticle size and surface chemistry determine serum protein adsorption and macrophage uptake, J. Am. Chem. Soc. 134 (2012) 2139–2147, https://doi.org/10.1021/ja2084338.
[59] Z.-T. Cao, L.-Q. Gan, W. Jiang, J.-L. Wang, H.-B. Zhang, Y. Zhang, Y. Wang, X. Yang, M. Xiong, J. Wang, Protein binding affinity of polymeric nanoparticles as a direct indicator of their pharmacokinetics, ACS Nano 14 (2020) 3563–3575, https://doi.org/10.1021/acsnano.9b10015.
[60] J.L. Perry, K.G. Reuter, M.P. Kai, K.P. Herlihy, S.W. Jones, J.C. Luft, M. Napier, J. E. Bear, J.M. DeSimone, PEGylated PRINT nanoparticles: the impact of PEG density on protein binding, macrophage association, biodistribution, and pharmacokinetics, Nano Lett. 12 (2012) 5304–5310, https://doi.org/10.1021/nl302638g.
[61] P. Aggarwal, J.B. Hall, C.B. McLeland, M.A. Dobrovolskaia, S.E. McNeil, Nanoparticle interaction with plasma proteins as it relates to particle biodistribution, biocompatibility and therapeutic efficacy, Adv. Drug Deliv. Rev. 61 (2009) 428–437, https://doi.org/10.1016/j.addr.2009.03.009.
[62] M.P. Monopoli, C. Åberg, A. Salvati, K.A. Dawson, Biomolecular coronas provide the biological identity of nanosized materials, Nat. Nanotechnol. 7 (2012) 779–786, https://doi.org/10.1038/nnano.2012.207.
[63] F. Chen, G. Wang, J.I. Griffin, B. Brenneman, N.K. Banda, V.M. Holers, D.S. Backos, L. Wu, S.M. Moghimi, D. Simberg, Complement proteins bind to nanoparticle protein corona and undergo dynamic exchange in vivo, Nat. Nanotechnol. 12 (2017) 387–393, https://doi.org/10.1038/nnano.2016.269.
[64] S. Schöttler, G. Becker, S. Winzen, T. Steinbach, K. Mohr, K. Landfester, V. Mailänder, F.R. Wurm, Protein adsorption is required for stealth effect of poly (ethylene glycol)- and poly(phosphoester)-coated nanocarriers, Nat. Nanotechnol. 11 (2016) 372–377, https://doi.org/10.1038/nnano.2015.330.
[65] M.A. Carignano, I. Szleifer, Prevention of protein adsorption by flexible and rigid chain molecules, Colloids Surf., B 18 (2000) 169–182, https://doi.org/10.1016/S0927-7765(99)00146-0.
[66] K.M. Tsoi, S.A. MacParland, X.-Z. Ma, V.N. Spetzler, J. Echeverri, B. Ouyang, S. M. Fadel, E.A. Sykes, N. Goldaracena, J.M. Kaths, J.B. Conneely, B.A. Alman, M. Selzner, M.A. Ostrowski, O.A. Adeyi, A. Zilman, I.D. McGilvray, W.C.W. Chan, Mechanism of hard-nanomaterial clearance by the liver, Nat. Mater. 15 (2016) 1212–1221, https://doi.org/10.1038/nmat4718.
[67] P. Grenier, I.M.O. Viana, E.M. Lima, N. Bertrand, Anti-polyethylene glycol antibodies alter the protein corona deposited on nanoparticles and the physiological pathways regulating their fate in vivo, J. Contr. Release 287 (2018) 121–131, https://doi.org/10.1016/j.jconrel.2018.08.022.
[68] M.D. McSweeney, T. Wessler, L.S.L. Price, E.C. Ciociola, L.B. Herity, J.A. Piscitelli, W.C. Zamboni, M.G. Forest, Y. Cao, S.K. Lai, A minimal physiologically based pharmacokinetic model that predicts anti-PEG IgG-mediated clearance of PEGylated drugs in human and mouse, J. Contr. Release 284 (2018) 171–178, https://doi.org/10.1016/j.jconrel.2018.06.002.
[69] K. Shiraishi, K. Kawano, Y. Maitani, T. Aoshi, K.J. Ishii, Y. Sanada, S. Mochizuki, K. Sakurai, M. Yokoyama, Exploring the relationship between anti-PEG IgM behaviors and PEGylated nanoparticles and its significance for accelerated blood clearance, J. Contr. Release 234 (2016) 59–67, https://doi.org/10.1016/j.jconrel.2016.05.010.
[70] B. Li, Z. Yuan, H.-C. Hung, J. Ma, P. Jain, C. Tsao, J. Xie, P. Zhang, X. Lin, K. Wu, S. Jiang, Revealing the immunogenic risk of polymers, Angew. Chem. Int. Ed. 57 (2018) 13873–13876, https://doi.org/10.1002/anie.201808615.
[71] J. McCallen, J. Prybylski, Q. Yang, S.K. Lai, Cross-reactivity of select PEG-binding antibodies to other polymers containing a C-C-O backbone, ACS Biomater. Sci. Eng. 3 (2017) 1605–1615, https://doi.org/10.1021/acsbiomaterials.7b00147.
[72] T. Shimizu, A.S.A. Lila, R. Fujita, M. Awata, M. Kawanishi, Y. Hashimoto, K. Okuhira, Y. Ishima, T. Ishida, A hydroxyl PEG version of PEGylated liposomes and its impact on anti-PEG IgM induction and on the accelerated clearance of PEGylated liposomes, Eur. J. Pharm. Biopharm. 127 (2018) 142–149, https://doi.org/10.1016/j.ejpb.2018.02.019.
[73] M.R. Sherman, L.D. Williams, M.A. Sobczyk, S.J. Michaels, M.G.P. Saifer, Role of the methoxy group in immune responses to mPEG-protein conjugates, Bioconjugate Chem. (2012) 485–499, https://doi.org/10.1021/bc200551b.
[74] A. Sunder, R. Hanselmann, H. Frey, R. Mülhaupt, Controlled synthesis of hyperbranched polyglycerols by ring-opening multibranching polymerization, Macromolecules 32 (1999) 4240–4246, https://doi.org/10.1021/ma990090w.
[75] D.Y. Joh, Z. Zimmers, M. Avlani, J.T. Heggestad, H.B. Aydin, N. Ganson, S. Kumar, C.M. Fontes, R.K. Achar, M.S. Hershfield, A.M. Hucknall, A. Chilkoti, Architectural modification of conformal PEG-bottlebrush coatings minimizes anti-PEG antigenicity while preserving stealth properties, Adv. Healthc. Mater. 8 (2019), 1801177, https://doi.org/10.1002/adhm.201801177.
[76] M.G.P. Saifer, L.D. Williams, M.A. Sobczyk, S.J. Michaels, M.R. Sherman, Selectivity of binding of PEGs and PEG-like oligomers to anti-PEG antibodies induced by methoxyPEG-proteins, Mol. Immunol. 57 (2014) 236–246, https://doi.org/10.1016/j.molimm.2013.07.014.
[77] J.T. Huckaby, T.M. Jacobs, Z. Li, R.J. Perna, A. Wang, N.I. Nicely, S.K. Lai, Structure of an anti-PEG antibody reveals an open ring that captures highly flexible PEG polymers, Commun. Chem. 3 (2020) 124, https://doi.org/10.1038/s42004-020-00369-y.
[78] N. Dagan, N. Barda, E. Kepten, O. Miron, S. Perchik, M.A. Katz, M.A. Hernán, M. Lipsitch, B. Reis, R.D. Balicer, BNT162b2 mRNA covid-19 vaccine in a nationwide mass vaccination setting, N. Engl. J. Med. 384 (2021) 1412–1423, https://doi.org/10.1056/NEJMoa2101765.
[79] L.R. Baden, H.M. El Sahly, B. Essink, K. Kotloff, S. Frey, R. Novak, D. Diemert, S. A. Spector, N. Rouphael, C.B. Creech, J. McGettigan, S. Khetan, N. Segall, J. Solis, A. Brosz, C. Fierro, H. Schwartz, K. Neuzil, L. Corey, P. Gilbert, H. Janes, D. Follmann, M. Marovich, J. Mascola, L. Polakowski, J. Ledgerwood, B.S. Graham, H. Bennett, R. Pajon, C. Knightly, B. Leav, W. Deng, H. Zhou, S. Han, M. Ivarsson, J. Miller, T. Zaks, Efficacy and safety of the mRNA-1273 SARS-CoV-2 vaccine, N. Engl. J. Med. 384 (2021) 403–416, https://doi.org/10.1056/NEJMoa2035389.
[80] M.C. Castells, E.J. Phillips, Maintaining safety with SARS-CoV-2 vaccines, N. Engl. J. Med. 384 (2020) 643–649, https://doi.org/10.1056/NEJMra2035343.